



Escola d'Enginyeria de Telecomunicació i
Aeroespacial de Castelldefels

UNIVERSITAT POLITÈCNICA DE CATALUNYA BARCELONATECH

MASTER THESIS

TITLE: Advanced Techniques for Optical Access Networks based on OFDM

MASTER DEGREE: Master of Science in Telecommunication Engineering & Management,
MASTEAM

AUTHOR: Blanca Arcas Serrate

DIRECTOR: PhD M^a Concepción Santos Blanco

DATE: October, 5th 2012

*Title: **Advanced Techniques for Optical Access Networks based on OFDM***

*Author: **Blanca Arcas Serrate***

*Director: **PhD M^a Concepción Santos Blanco***

*Data: **October, 5th 2012***

Overview

This Master Thesis aims to review and study the different alternatives for application of OFDM technologies to optical fibre networks and assess their potential as the basis of the next generation PON. **New proposals based on predistortion circuits** which alter the OFDM signal to transmit prior to optical modulation will be made and analyzed.

A total of 6 different systems have been designed and their performance assessed through numerical simulations. These systems are composed by predistortion and conventional oIQ transmitters joined with Direct Detection (DD), Basic Heterodyne Coherent Detection and Conventional Homodyne Coherent Detection, (COHD) receivers.

All the simulations have used the commercial software VPItransmissionMaker™ and VPIphotonicsAnalyzer™, (VPI) in combination with Matlab coding for the OFDM coder and decoder.

The performance of 6 optical OFDM transmission system scenarios is measured by running a script in TCL/TK language that allows to run a simulation sequence in which the parameters under study such as Sensitivity and Extinction Ratio (ER) were successively changed in order to obtain informative plots about the systems transmission properties.

INDEX

Introduction	1
Chapter 1. Background	5
1.1 Optical OFDM.....	5
1.1.1 OFDM Basic Principles	5
1.2 Optical Communications	8
1.2.1 Intensity Modulation / Direct Detection System	8
1.2.2 Optical Basic Devices	9
Chapter 2. OFDM for Optical Networks	17
2.1 Optical OFDM Systems	18
2.1.1 Transmitter	18
2.1.2 OFDM Receiver.....	23
2.2 OFDMA PON	26
Chapter 3. Simulations Background	29
3.1 Simulation's Tool	29
3.1.1 Embedded Modules Used	29
3.2 OFDM Modules	31
3.2.1 OFDM Coder	31
3.2.2 OFDM Decoder	31
3.3 Universe Setting Parameters	32
Chapter 4. Optical OFDM Simulated Systems	35
4.1 Ideal Predistortion Systems in VPI – 1 st Step	35
4.2 Real Predistortion Systems in VPI – 2 nd Step.....	36
4.3 Conventional oIQ Systems in VPI – 3 rd Step.....	37
4.4 Predistortion Systems Description.....	39
4.4.1 System A ₁	39
4.4.2 System B ₁	41
4.4.3 System C ₁	43
Chapter 5. Summary of Results	45
5.1 Sensitivity versus Fibre Length	45
5.2 ER variation	46
Chapter 6. Environmental Impact.....	49
Chapter 7. Conclusions	51
Acronyms	53
Bibliography.....	55
ANNEXES	57
A. Diode Laser Definition	57

<i>Stimulated Emission</i>	57
<i>Linewidth and Monochromatic Light Generation</i>	58
B. PIN Photodiode	59
C. oIQ Systems.....	60
<i>oIQ / Hybrid 90° COHD B2B System's Description</i>	60
<i>oIQ plus SSB modulated Tone / DD: B2B System's Description</i>	61
<i>oIQ / Basic Heterodyne COHD: B2B System's Description</i>	63
<i>oIQ Results: Systems A₂ / B₂ / C₂</i>	64
D. Tcl/tk Script	67

Index of Figures

Figure 1.1 Spectrum of WDM/FDM and OFDM, respectively [6]	5
Figure 1.2 IFFT Module scheme at the transmitter side	6
Figure 1.3 Effect of Chromatic Dispersion over OFDM symbol with CP [7]	6
Figure 1.4 General OFDM Transmitter Scheme [7]	7
Figure 1.5 General OFDM Receiver Scheme [6]	7
Figure 1.6 Optical output power versus current in a laser diode	8
Figure 1.7 Lorentzian's function representation	9
Figure 1.8 Optical Losses vs Wavelength Graph [13]	10
Figure 1.9 Chromatic Dispersion vs Wavelength [13]	11
Figure 1.10 Mach – Zehnder Modulator Scheme	12
Figure 1.11 MZM Transfer Functions	13
Figure 1.12 Input and Output signals in QP of MZM	13
Figure 1.13 VPI Setting Parameters of Predistortion Systems	14
Figure 1.14 Setting Parameters of conventional oIQ Systems	14
Figure 1.15 Hybrid 90° Scheme	15
Figure 2.1 Optical Systems Classification	18
Figure 2.2 oIQ OFDM Transmitter	19
Figure 2.3 Predistortion's Scheme with a DD-MZM	20
Figure 2.4 oIQ with SSB Tone	23
Figure 2.5 Direct Detection Receiver Scheme	24
Figure 2.6 Basic Heterodyne Coherent Detection Scheme	24
Figure 2.7 Basic Homodyne Coherent Detection Scheme	25
Figure 2.8 Homodyne Conventional Coherent Detection Receiver Scheme	25
Figure 2.9 Heterodyne Conventional Coherent Detection Receiver Scheme	26
Figure 2.10 Basic PON structure scheme	26
Figure 3.1 OFDM Coder Galaxy in VPI	31
Figure 3.2 OFDM Decoder Galaxy in VPI	31
Figure 3.3 Universe Setting Parameters	32
Figure 4.1 Ideal Predistortion Transmitters in VPI with and without SSB Tone generation	35
Figure 4.2 Constellation Diagram of Ideal Predistortion Systems A1, B1 and C1, respectively. With BER=0, infinite ER and fibre length not considered	36
Figure 4.3 Internal Block of the Real Predistortion Module and CoSimInterface internal parameter.....	36
Figure 4.4 Conventional oIQ Transmitters in VPI with and without SSB Tone generation	37

Figure 4.5 Constellation Diagram of Conventional oIQ Systems A2, B2 and C2, respectively. With BER=0, infinite ER and fibre length not considered	38
Figure 4.6 System A1 Scheme	39
Figure 4.7 System A1 VPI's Scheme	39
Figure 4.8 System A ₁ : θ_{1t} predistortion signal	40
Figure 4.9 System A ₁ : θ_{2t} predistortion signal	40
Figure 4.10 System A ₁ : $X_o(f_{REF})$ with -49.38 dBm	40
Figure 4.11 System A ₁ : $R_{e_I}(f_B)$	40
Figure 4.12 System A ₁ : Constellation Diagram, BER =0	40
Figure 4.13 OFDM System B1 Scheme	41
Figure 4.14 System B1 VPI's Scheme	41
Figure 4.15 System B ₁ : θ_{1t} predistortion signal	42
Figure 4.16 System B ₁ : θ_{2t} predistortion signal	42
Figure 4.17 System B ₁ $X_o(f_{REF})$ with -49.38 dBm	42
Figure 4.18 System B ₁ : $R_{e_I}(f_C)$	42
Figure 4.19 System B ₁ : Constellation Diagram, BER=0	42
Figure 4.20 System C1 Scheme	43
Figure 4.21 System C1 in VPI's Scheme (I)	43
Figure 4.22 System C ₁ : $X_o(f_{REF})$	44
Figure 4.23 System C ₁ : $X_o(f_{REF})$ plus the auxiliary carrier at 15 GHz from $X_o(f_{REF})$	44
Figure 4.24 System C ₁ : $R_{e_I}(f_B)$	44
Figure 4.25 System C ₁ : Constellation Diagram, BER=0	44
Figure 5.1 Sensitivity vs Length Systems A1, C1, A2, and C2	45
Figure 5.2 Sensitivity vs Length Systems B1 and B2	46
Figure 5.3 Constellation Diagram of Conventional oIQ Systems A2, B2 and C2, respectively. With BER=0.00188, ER=30 and fibre length not considered	46
Figure 5.4 Constellation Diagram of Real Systems A1, B1 and C1, respectively. With BER=0, ER=30 and fibre length not considered	47
Figure 5.5 BER vs ER representation	47
Figure 5.6 System A ₁ : Sensitivity vs Fibre Length representation	47
Figure 5.7 System A ₁ : Sensitivity vs Fibre Length representation	47
Figure 5.8 System B ₁ : Sensitivity vs Fibre Length representation	48
Figure 5.9 System B ₁ : BER vs Fibre Length representation	48
Figure 5.10 System B ₁ : Sensitivity vs Fibre Length representation	48
Figure 5.11 System B ₁ : BER vs Fibre Length representation	48
Figure 0.1 Stimulated Emission's Scheme	57
Figure 0.2 Detailed Fabry-Perot semiconductor laser Scheme	58
Figure 0.3 Photon flux passing through photodiode material	59
Figure 0.4 Energy-band's diagram for pin photodiode	59
Figure 0.5 OFDM oIQ with Homodyne Hybrid 90° Coherent Detection Scheme	60
Figure 0.6 OFDM oIQ with Homodyne Hybrid 90° Coherent Detection Scheme in VPI	60
Figure 0.7 System A: $X_{e_I}(f_B)$	61
Figure 0.8 System A: $X_o(f_{REF})$	61
Figure 0.9 System A: $R_{e_I}(f_B)$	61
Figure 0.10 System A: Constellation Diagram, BER=0	61
Figure 0.11 OFDM oIQ plus SSB modulated Tone with Direct Detection Scheme	61
Figure 0.12 OFDM oIQ plus SSB modulated with Direct Detection Scheme in VPI	62
Figure 0.13 System B: $X_{e_I}(f_B)$ & SSB tone at 15GHz	62
Figure 0.14 System B: $X_o(f_{REF})$	62
Figure 0.15 System B: $R_e(f_B)$	63

Figure 0.16 System B: Constellation Diagram, BER=0.....	63
Figure 0.17 OFDM oIQ with Basic Heterodyne Coherent Detection Scheme	63
Figure 0.18 OFDM oIQ with Heterodyne Coherent Detection Scheme	63
Figure 0.19 System C: $X_o(f_{REF})$	64
Figure 0.20 System C: $X_o(f_{REF})$ plus the auxiliary carrier at 15 GHz from $X_o(f_{REF})$	64
Figure 0.21 System C: $R_e(f_B)$	64
Figure 0.22 System C: Constellation Diagram	64
Figure 0.23 System A2: Sensitivity vs Length representation	65
Figure 0.24 System A2: BER vs Length representation	65
Figure 0.25 System B2: Sensitivity vs Fibre Length representation	65
Figure 0.26 System B2: Sensitivity vs Fibre Length representation	65
Figure 0.27 System C2: Sensitivity vs Fibre Length representation	65
Figure 0.28 System C2: BER vs Fibre Length representation	65
Figure 0.29 System A: $X_o(f_{REF})$ and Eye Diagram, BER=0.00188	66
Figure 0.30 System B: $X_o(f_{REF})$ and Eye Diagram with BER=0.00187	66
Figure 0.31 System C: $X_o(f_{REF})$ and Eye Diagram with BER=0.00187	66

Index of Tables

Table 2.1 Downstream Systems.....	26
Table 2.2 Upstream Systems	27
Table 2.1 VPI embedded Modules used	30

Introduction

Broadband communication has become a requirement in the present days due to the social change related with the Web 2.0 introducing the information revolution at all levels. In few years there has been a massive increase of users, devices connected to the internet and so an unstoppable growth of information's interchange.

Through this evolution many technologies have been studied in order to provide the necessities demanded by the market. Furthermore it has to be noted the different type of users in order to satisfy diverse service requirements. There will coexist in common network different types of technologies, depending on the environments. In general mobile communications in a free space or radiofrequency environment and fixed point communications are distinguished. In the first environment a hybrid network will be necessary (using RF technologies in the access network such as 3G, TETRA, Wi-Fi, WiMAX, LTE, LOS Radiolinks and optical communications in the metro and core network) and in the second environment its current development goes towards a complete optical communication network due to its high rates achievements.

This project will be focused on the second type of environment where currently Passive Optical Networks (PON) are deployed to substitute conventional cable-based access networks. It uses optical fibre as transmission media and offers much higher bandwidth while supporting various communication services, basically is a point-to-multipoint topology. The first modern PON networks deployed were based on TDMA and standardized by the ITU as Broadband PON (BPON); newer TDMA deployments are typically based on either Gigabit-Capable PON or GPON (ITU-T 984) and Ethernet PON or EPON (IEEE 802.3ah)[1].

In general these PON standards are bounded by their adaptability in different terms taking into account the exponential capacity's demand of the new type of society. They have a maximum nominal line rate of 2.4 Gbit/s (upstream/downstream), all 3 standards allow for a passive split ratio of 1:16 or higher, with 1:32 being the most popular ratio deployed and the maximum distance from the head end to the subscribers is generally 20 km [2].

New Generation or NGPON systems have the aim of improving the above limitations introducing better scalability and adaptability for present technologic development. There have appeared different technologies meeting some of the requirements such as 10GPON and WDM-PON but OFDMA-PON has many advantages compared to the other PON technologies (being still challenges to overcome).

OFDMA-PON has scalable architecture (capable of coexisting with TDM-PON and WDM-PON), improved bandwidth efficiency (assigning different subcarriers to multiple users in a dynamic manner), protocol independence, service transparency and cost-effective solutions. One of the best features of OFDM is its ability for compensating the channel linear impairments such as the chromatic dispersion in optical fibre. A training sequence added at the transmitter is capable of correcting the received data successfully [3].

This master thesis is inside the frame of the Accordance Project, funded by the EU. It has the aim of investigating the introduction of OFDMA into a PON architecture offering at the same time optical backhauling for wireless and copper-based networks [4].

The advent of OFDM into optical communications is quite recent. Reasons for the late embracement of such a successful format in other applications can be found in that performances required were perfectly within reach of optical fibre systems without having to resort to very complex modulation formats, in the fact that type of digital signal processing at the required speed was not available then and also because as we will be seeing conventional optical transmission systems do not fit well with conventional OFDM systems.

Moreover in recent publications it has been proposed as an attractive modulation format for long-haul transmission either in coherent detection (section 2.1.2.2) or in direct detection (section 2.1.2.1) [8].

But it has to be noted that one of its pro tem drawbacks is the complexity OFDM requires due to the implementation of IFFT/FFT algorithms. They have to be processed in a DSP (Digital Signal Processor) and as well the use of DAC/ADC is needed, altogether rising the system's price. It is a pro tem drawback because when implementing a DSP leads to introduce many improvements in an electronic way as they could be digital filters and other required digital modules. They may redeem the first inversion as well as reducing the price in future system's extensions. An important bonus for OFDM is its successful application and very fast growth in wireless technologies such as WiMAX and LTE.

Basically two trends may be identified, one aims at transforming OFDM systems to fit into an IM/DD conventional optical transmission system, by for example imposing the Hermitian Symmetry property or by inserting an electrical IQ stage, and the other consists on transforming the optical systems to fit into the OFDM technology, that would be the use of Amplitude modulation by for example allocating a guardband or by using optical IQ modulation and coherent detection. [11][12].

In this thesis work the goal is to review and study the different alternatives for application of OFDM technologies to optical fibre networks and assess their potential as the basis of the next generation PON. Besides options described in the literature, ***new proposals based on predistortion circuits*** which alter the OFDM signal to transmit prior to optical modulation will be made and analyzed.

Furthermore the analytical basis and structure of the predistortion circuits will be developed and 6 implemented and simulated scenarios, that confirm a proper behaviour of predistortion systems, will be seen throughout the document.

The thesis dissertation is divided in five main chapters, all of them containing the following structure and concepts:

Chapter 1 starts with an introduction to the required background in optical OFDM and optical communications in order to be able to understand the different concepts related with the analysed, designed and assessed optical systems.

Chapter 2 devotes to describe the OFDM for optical systems used throughout the master-thesis splitting the system in transmitters and receivers. An important section (2.1.1.2) is the one containing the mathematical process to obtain the predistortion expressions, basis for the new proposed modulation.

Chapter 3 is an introduction to the simulation's tool, based on a combination of Matlab code modules embedded into the optical systems block simulator Virtual Photonics Inc.(VPI), focused on the OFDM coder/decoder modules and on the general setting parameters of the implemented systems.

Chapter 4 describes the process for the implementation and assessment of the real predistortion systems. This process starts from ideal predistortion systems to the implementation of the conventional oIQ systems in order to check and compare the obtained predistortion results. The main section is focused on the back to back (B2B) real predistortion system's description with general schemes and signal's images at the different stages.

Chapter 5 sets forth the different results obtained. First a comparison between predistortion and conventional oIQ systems regarding sensitivity versus fibre length is done. Next the systems' behaviour is shown when changing ER value.

Chapter 6 discusses the environmental impact of the work developed and finally chapter 7 includes a summary of conclusions and an overview about possible future lines of research.

Chapter 1. Background

This chapter comprises a revision of basic definitions related to both OFDM systems and optical communications.

1.1 Optical OFDM

This section will be a review of basic concepts of Orthogonal Frequency Division Multiplexing, OFDM.

1.1.1 OFDM Basic Principles

OFDM's fundamental principle is to decompose the high rate data stream into N lower rate streams and then transmitting them simultaneously over a large number of subcarriers [5]. The choice of individual subcarrier is such that they are orthogonal to each other by fulfilling the orthogonality condition (1.1):

$$\Delta f = \frac{1}{N \cdot T_S} = \frac{1}{T_N} \quad (1.1)$$

Expression (1.1) describes the separation between subcarriers, Δf , in order to be orthogonal to each other. This depends on the number of subcarriers N and the period of a symbol, T_S [3]. The highest the N , the narrower the Δf . The subcarriers' bandwidth is conveniently chosen so that every subcarrier individually experiences flat fading through the dispersive channel.

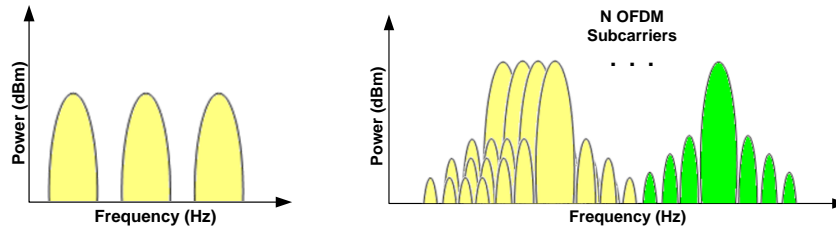


Figure 1.1 Spectrum of WDM/FDM and OFDM, respectively [6]

Figure 1.1 shows the comparison between the WDM/FDM spectrum, where the required frequency band gap between carriers is seen, and OFDM spectrum, where overlapping results in a better spectral efficiency hence achieving superior bandwidth utilization [5]

In section 1.1.1.1 is described mathematically the process of converting 4QAM symbols (digital modulation used in the simulations of the different systems) into an OFDM symbol, and vice versa.

1.1.1.1 OFDM Modulation/Demodulation

Obtaining an OFDM signal at the transmitter side requires the implementation of IFFT algorithm with a discrete input signal. The expression (1.2) defines the IFFT of a complex symbol C_e over the k th subcarrier:

$$s_n = \frac{1}{\sqrt{N}} \cdot \sum_{k=0}^{N-1} C_e^k \cdot e^{j\frac{2\pi}{N}kn}; \quad [0 \leq n \leq N-1] \quad (1.2)$$

Where s_n is the discrete resultant signal defined from $n = 0$ to $n = N - 1$ and N is the total number of orthogonal subcarriers generated.

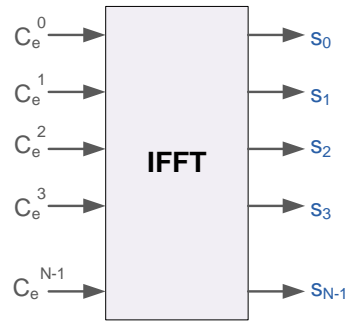


Figure 1.2 IFFT Module scheme at the transmitter side

In Figure 1.2 the IFFT module with its inputs and outputs as defined in (1.2) is graphically represented. By fulfilling the orthogonality condition (1.1) when executing the IFFT algorithm results in the generation of OFDM symbols composed of 4QAM symbols over N orthogonal subcarriers.

Moreover OFDM demodulating process is based, among other operations, on the implementation of the FFT algorithm at the receiver side, as shown in (1.3).

$$C_e^k = \frac{1}{\sqrt{N}} \cdot \sum_{n=0}^{N-1} S_n \cdot e^{-j\frac{2\pi}{N}kn}; \quad [0 \leq k \leq N-1] \quad (1.3)$$

The resultant signal in (1.3) is composed by the original group of 4QAM symbols defined from the subcarriers $k = 0$ to $k = N - 1$ [6]. In this case any possible effect from the channel is ignored.

1.1.1.2 Cyclic Prefix

The orthogonality of subcarriers is maintained even in the time-dispersive channel by adding the Cyclic Prefix or CP [5]. The OFDM symbol is extended by copy-pasting the beginning of the symbol to the end (or vice versa) before transmission; when receiving it has to be subtracted before FFT module [7].

Although it introduces some redundancy reducing the overall data rate, CP eliminates both Inter-Symbol Interference (ISI) and Inter-Carrier Interference (ICI) from the received signal being the key to simple equalization in OFDM. [6].

In order to take the ISI problem out, CP has to be longer than the delay spread of the channel. The other named problem was the ICI effect. This is a penalty due to the incomplete OFDM waveform caught by the DFT window. It can be solved just by adding the guard band or CP thanks to the periodicity of the FFT [3].

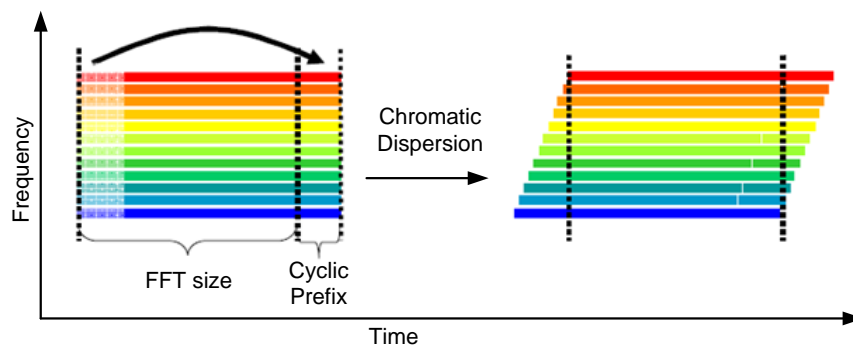


Figure 1.3 Effect of Chromatic Dispersion over OFDM symbol with CP [7]

Figure 1.3 shows the effect of dispersion introduced by the channel over the OFDM symbol. Something important to have into account at the receiver side is the necessity of integrating it over a length equal to the FFT size [7]. As well from this figure is observed the created matrix ($N_c \times n_{S_{OFDM}}$) when modulating an OFDM signal, where N_c are the different orthogonal subcarriers and $n_{S_{OFDM}}$ are the different OFDM symbols generated.

1.1.1.3 Transmitter and Receiver Modules

There are many steps in order to obtain an OFDM signal. In Figure 1.4 is shown these required operations from the input data until a base band OFDM signal is obtain (split in inphase and quadrature components).

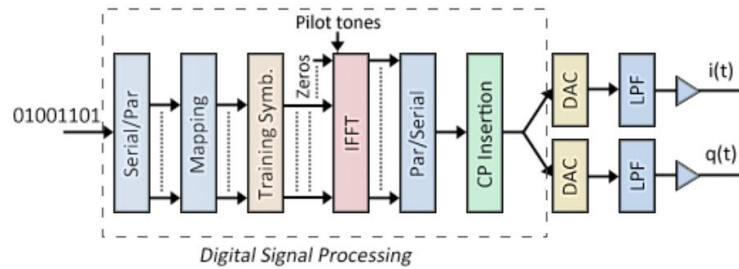


Figure 1.4 General OFDM Transmitter Scheme [7]

Mapping process is when converting bits into symbols. Then a training sequence is introduced for estimating the channel response and calculating the equalizer coefficients at the receiver. Following the IFFT algorithm is executed (with or without zero-padding). When the signal is transformed from parallel to serial the CP is inserted. At the end each of the signal's components goes through a DAC (Digital/Analog Converter) and a LPF (Low Pass Filter). From this step the electrical OFDM signal would be optically modulated in a radiofrequency to optical (RTO) system and sent through the optical fibre.

Once the optical signal reaches the receiver side an optical system to convert from optical to radiofrequency, OTR, is required. Then the signal would entry In Figure 1.5 where an OFDM receiver is shown. These two components of the received signal would go through the reverse process applied at the transmitter side. First the LPF and DAC would be applied (respectively). After that, an OFDM symbol synchronization process is required before the CP is removed. Then the signal is ready to be introduced in the FFT algorithm. Next, the training sequence is removed from the electrical received signal and sent to the channel estimation process. The electrical signal's equalization process, at this point, takes the estimation of the channel and sets its internal values to compensate errors in the received signal. When optical coherent receivers are employed, before recovering the original signal the phase noise introduced through the system has to be compensated.

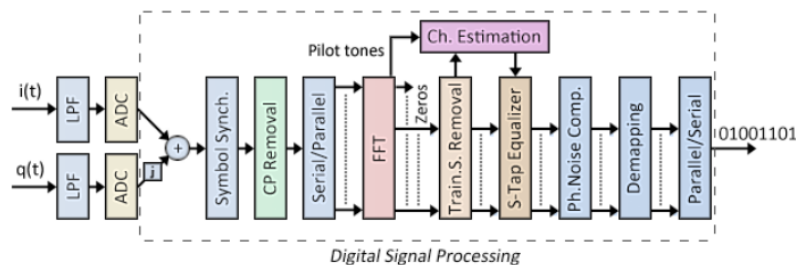


Figure 1.5 General OFDM Receiver Scheme [6]

The optical modulator/demodulator stages (RTO/OTR) define each of the different optical OFDM alternatives that at the present time are being studied which are discussed in Chapter 2.

1.2 Optical Communications

Since optoelectrical conversions are based on interchanges between electrons and photons the most natural way of modulating a signal on an optical carrier is to make the intensity of the light to follow the signal variations. The reverse process in the receiver converts the optical intensity in an electrical current usually in a photodiode. This is known as IM/DD systems. However, when linear optical impairments such as CD alter the transmitted signal nonlinear distortions arise.

In section 1.2.1 the basic features of IM/DD systems are explained and following sections describe basic optical devices.

1.2.1 Intensity Modulation / Direct Detection System

Intensity Modulation is based on varying the laser drive current with the data packet on the electrical domain producing a variation on the optical output power. So the signal is modulated on the electrical domain according to the expression (1.4):

$$P_{out}(t) = P_o \cdot (1 + m \cdot s(t)) \quad (1.4)$$

Where $P_{out}(t)$ is the time varying optical output power, P_o is the average optical output power or optical carrier power, $s(t)$ is the time-varying electric analog signal (used to modulate an optical source directly about bias current point I_B) and m is the modulation index defined in laser diodes as (1.5):

$$m = \frac{\Delta I}{I_B - I_{th}} \quad (1.5)$$

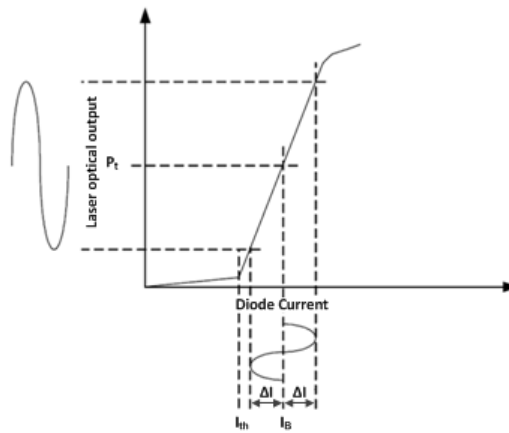


Figure 1.6 Optical output power versus current in a laser diode

With I_B the DC bias applied to the laser's driving signal, I_{th} the laser's current threshold and ΔI the maximum information signal excursion or dynamic range.

In order to reduce distortion of the whole system, modulation must be fitted on the linear part of the curve as shown in Figure 1.6 by regulating the m value.

At the receiver side the complementary function, performed by a photodiode will recover the electrical information signal as a detected photocurrent, $I_R(t)$, proportional to the intensity of the received optical signal, with $E_R(t)$ the amplitude of the electrical field associated to the optical wave.

$$E_R(t) \propto \sqrt{I_R(t)} \quad (1.6)$$

A drawback comes when turning the laser *on* and *off* with an electrical drive current, it produces the phenomenon referred as *chirp* (widening of laser bandwidth). It makes directly modulation lasers undesirable for operation at data rates greater than about 2.5 Gb/s [1].

1.2.2 Optical Basic Devices

1.2.2.1 Diode Laser

Semiconductor diode lasers are used as the light source in optical communication systems. Distributed Feedback lasers (DFB) present the best performance-cost trade-off, while more expensive External Cavity Lasers (ECL) can be found in more advanced applications (such as coherent receivers) due to its very small phase noise.

When simulating the different systems in this thesis, the value used as linewidth in the different lasers has been 1kHz. The reason for using such small value has been to avoid any possible effect due to the introduction of phase noise in the system, since phase noise compensation is beyond the thesis's goals. The other parameter introduced in the simulated lasers is the output power; it has been fixed to 5mW in order to avoid non linearities.

Commonly the spectral curve of a single mode laser is represented by a Lorentzian function. It is defined in equation (1.7):

$$g(\nu) = \frac{\Delta\nu^2}{(\nu - \nu_0)^2 + \left(\frac{\Delta\nu}{2}\right)^2} \quad (1.7)$$

Figure 1.7 is a representation of the Lorentzian function $g(\nu)$ where the important parameters of the equation (1.7) are shown.

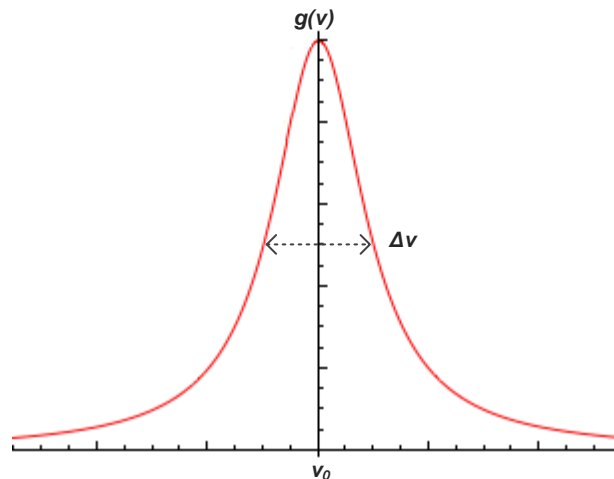


Figure 1.7 Lorentzian's function representation

1.2.2.1.1 Modulation of light

The most simple and cost-effective way of light modulation is the direct modulation of the driving current of the diode laser. While the external modulation provides better performances, it is also more expensive and difficult to operate and maintain and it is presently proposed for use in central offices where the cost may be shared by the multiple users supported.

For the purposes of this thesis, where we aim at demonstrating a new kind of modulation that uses predistortion, we will be mainly considering external modulation through electro-optical modulators. The basis of this kind of modulation is explained in Chapter 2.

1.2.2.2 Optical Fibre

The optical fibre is the transmission media where the light signals are transported and guided from source to destination, end to end.

The lasers deployed in optical communications typically operate at or around 850 nm (first window), 1310 nm (second window), and 1550 nm (third and fourth windows).

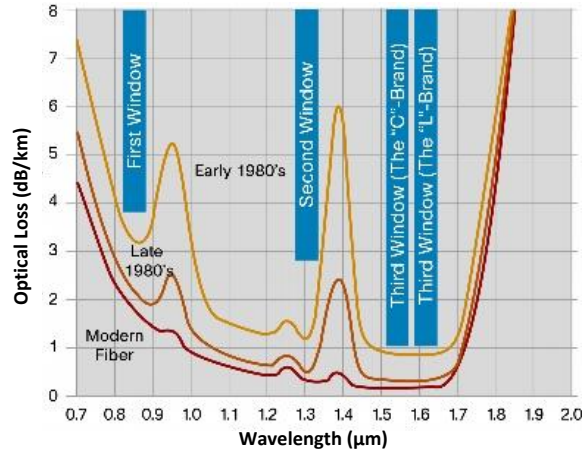


Figure 1.8 Optical Losses vs. Wavelength Graph [13]

Figure 1.8 shows the different wavelength windows considered for optical transmission. As it can be seen in the red curve, at the third window is where there are less optical losses, therefore it will be the window used in the simulated systems of this thesis.

The systems used in this thesis are located into the third window with a lambda $\lambda = 1550 \text{ nm}$ referring to a reference frequency of:

$$\lambda = \frac{c}{f} \rightarrow f_{REF} = \frac{c}{\lambda} = \frac{3 \cdot 10^8 \frac{m}{s}}{1550 \text{ nm}} = 193.5483 \text{ THz} \quad (1.8)$$

➤ Chromatic Dispersion

Chromatic dispersion (CD) originates from the fact that within the same mode, each wavelength travels at a slightly different velocity in a fibre, and thus they arrive at different times at the fibre end. Therefore, the range of arrival times at the fibre end of the spectrum of wavelengths will lead to pulse spreading.

The accumulated chromatic dispersion increases with distance along a link. It should be less than a fraction ε of the bit period $Tb = 1/B$ where B is the bit rate. Equation (1.9) gives the relationship [14]:

$$|D_{CD}| \cdot L \cdot \sigma_\lambda < \varepsilon \quad (1.9)$$

Where $|D_{CD}|$ is the Chromatic Dispersion in ps/(nm·km), L is the fibre length, σ_λ is the optical signal spectral width and ε is the power penalty requirement fixed by ITU-T. As shown in Figure 1.9, the typical chromatic dispersion around the third window in the standard single-mode NDSF (Non-Dispersion-Shifted Fibre) is 17 ps/(nm·km) .

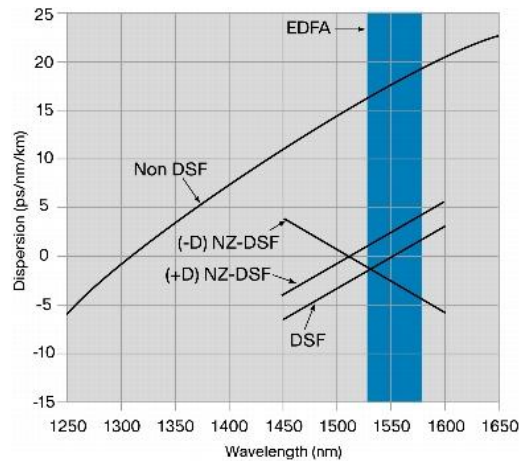


Figure 1.9 Chromatic Dispersion vs Wavelength [13]

1.2.2.3 Photodiode

At the output of an optical transmission line there must be a receiving device that interprets the information contained in the optical signal. A photodetector is the first element of the receiver system.

There exist different types of photodetectors but the one that meets the requirements for the fibre optical systems is the **photodiode** or semiconductor-based photoconductor.

The benefits of photodiodes are small size, suitable material, high sensitivity and fast response time. In optical communications, basically two types of photodiodes are used: PIN and Avalanche (APD) photodiodes. The one used in the simulations is the PIN photodiode, more information about this type of photodiodes in annex B [14].

For the purposes of our work the photodiode can be simply described as a device at whose output a photodetected current proportional to the optical signal intensity (squared modulus of amplitude electrical field) is found.

1.2.2.4 Mach-Zehnder Modulator (MZM)

Achieve a high digital bit rate modulation over the optical domain by the electro-optic effect, EO, is possible. The EO effect is defined as the variation of the optical refractive index of some materials such as the Lithium Niobate (LiNbO_3) when an electric field is applied. That gives rise to an optical phase modulation which can be converted to amplitude modulation by using an interferometric configuration such as a Mach Zehnder interferometer.

1.2.2.4.1 Operating Principle

An integrated MZM is formed by two opposing and bonded joints through two parallel branches. Each of the branches has metal electrodes in order to produce a relative phase shift $\Delta\phi$ through the EO effect, Figure 1.10.

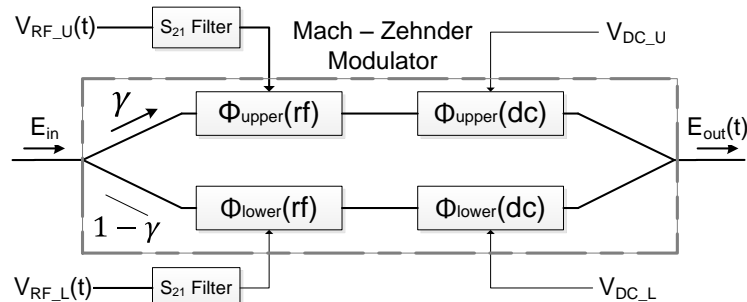


Figure 1.10 Mach – Zehnder Modulator Scheme

As shown in (1.10) the output electrical field of a MZM is the input electrical field multiplied by the impulse response or transfer function $h(t)$ of the same external modulator. It has to be noted that E_{in} is the electrical field of the coherent light beam generated by the input laser and $E_{out}(t)$ is the combination of the optical and electrical signals in each of the branches.

$$E_{out}(t) = E_{in} \cdot h(t)^2 \quad (1.10)$$

The internal impulse response has as inputs two different voltages, on the one hand the voltages referring to the electrical signal being later optically modulated and on the other hand the dc bias voltage. In Figure 1.10 is seen each of the MZM branches with their correspondent inputs. Likewise these voltages are internally converted to phases by the following expression (in radians):

$$\phi_{RF_U}(t) = \frac{\pi}{v_{\pi}} \cdot V_{RF_U}(t) \quad \phi_{RF_L}(t) = \frac{\pi}{v_{\pi}} \cdot V_{RF_L}(t) \quad (1.11)$$

$$\phi_{DC_U} = \frac{\pi}{v_{\pi}} \cdot V_{DC_U} \quad \phi_{DC_L} = \frac{\pi}{v_{\pi}} \cdot V_{DC_L} \quad (1.12)$$

Where V_{π} is a MZM's figure of merit referring to the voltage for π phase shift, then the resultant internal impulse response is obtained:

$$h(t) = e^{j(\phi_{DC_U} + \phi_{RF_U}(t))} + \gamma \cdot e^{\pm j(\phi_{DC_L} + \phi_{RF_L}(t))} \quad (1.13)$$

In expression (1.13) a new parameter, γ , appears. It indicates the weight of the optical signal to be distributed in each of the MZM's branches. When this parameter is 1 it means that the distribution is equitable between branches. It is important to notice that γ is related to the MZM Extinction Ratio (ER) specifying the difference between the maximum and minimum optical power at the MZM output. Their relation is shown in the following equation (in linear scale):

$$ER = \left(\frac{1+\gamma}{1-\gamma} \right)^2 \quad (1.14)$$

In addition both parameters are linked to the technological processes in the optical guides embedded into the EO crystal. Typical ER values are around 15-40 dB, a greater ER implies a better performance of the MZM in terms of achievement of deeper modulation depths and also a higher manufacturing cost.

Moreover usually the MZM is operated at two different biasing points, quadrature point (QP) and null point (NP) both of them shown in the transfer function of the MZM, Figure 1.11.

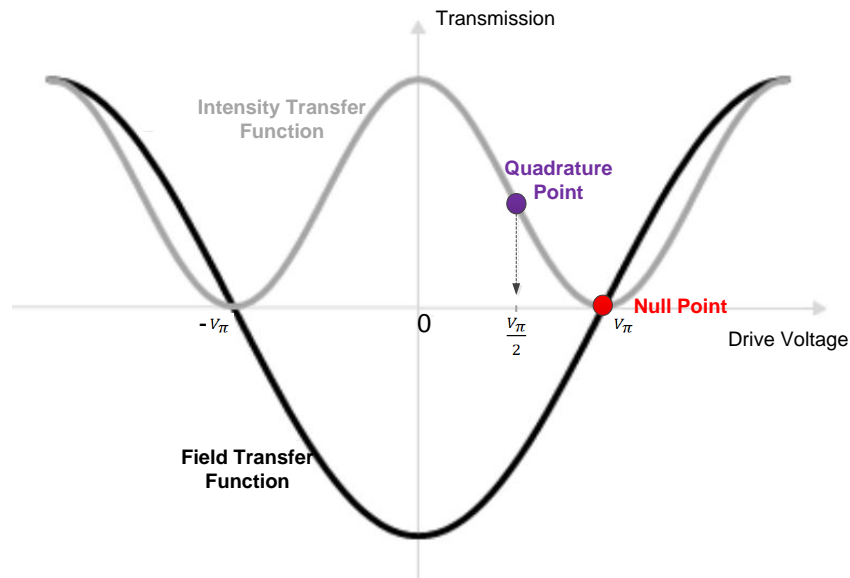


Figure 1.11 MZM Transfer Functions

As seen in the image, both points are located in the zones where the transfer function's linearity is maximal (referring respectively to the intensity transfer function, grey graph, in QP and to field transfer function in NP, black graph). Therefore the resultant signal's linearity is guaranteed. The required drive voltages to work on QP and NP are $\frac{V_\pi}{2}$ and V_π respectively. Figure 1.12 shows an example of the internal process of a MZM when operated at QP.

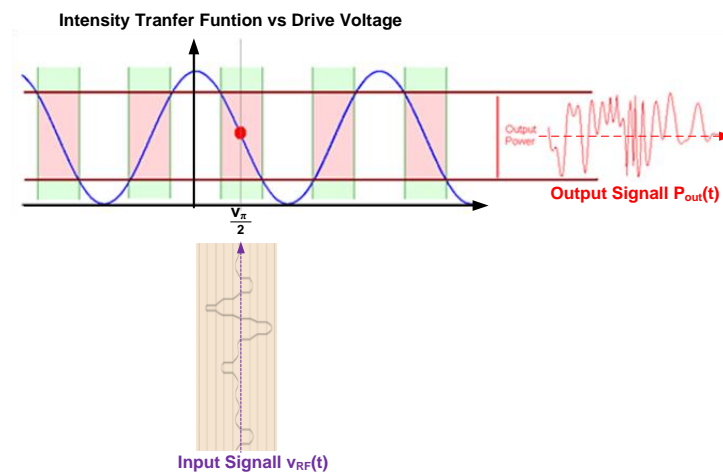


Figure 1.12 Input and Output signals in QP of MZM

It is important to notice that the optical carrier injected in the MZM will be affected by the operating point. In the case the MZM works in the QP, the optical carrier will be visible through the system and so it would be possible, if required, to take it into account such as for example when using a Direct Detection (DD) receiver.

On the other hand if the operating point is the NP then the injected optical carrier will be cancelled and therefore if other techniques, as the addition of auxiliary carriers, will have to be considered to deal with the fact of not having optical carrier when demodulating with a DD receiver.

In this master thesis MZM is the main component of the RTO module in the two implemented transmitters, ***predistortion*** and ***conventional oIQ***. Both have in common the same operating point, NP, therefore using the MZM's field transfer function.

- Firstly MZM has been the key for calculating the predistortion functions. When implementing **predistortion systems** into the VPI (simulation's tool) some special parameters were fixed. These parameters are listed in Figure 1.13.

Name	Value	Unit
Physical		
VpiDC	Vpi	V
VpiRF	Vpi	V
InsertionLoss	0	dB
ExtinctionRatio	ER	dB
LowerArmPhaseSense	POSITIVE	

Figure 1.13 VPI Setting Parameters of Predistortion Systems

As seen in the image LowerArmPhaseSense is valued as POSITIVE, this specifies for a given applied voltage, the phase change in the MZ's lower arm is the same sign as the upper arm. As well the Vpi (v_{π}) value denotes the NP operating point, its value is externally defined and fixed to π .

That Vpi choice allows simplifying the mathematical expression of the predistortion circuits. Another important parameter which does not appear in the above figure is the dc source, both V_{DC_U} and V_{DC_L} are fixed to 0v.

- The **conventional oIQ** setting parameters are outlined in Figure 1.14. Two MZM are required inside the RTO module, with LowerArmPhaseSense set to NEGATIVE meaning the phase sign in the lower arm is the opposite of the upper one.

In conventional oIQ the Vpi value has been fixed to 1v.

Name	Value	Unit
Physical		
VpiDC	Vpi	V
VpiRF	Vpi	V
InsertionLoss	0	dB
ExtinctionRatio	ER	dB
LowerArmPhaseSense	NEGATIVE	

Figure 1.14 Setting Parameters of conventional oIQ Systems

1.2.2.5 Hybrid 90°

The demodulation of coherent optical signals requires the combination of the received signal with a local oscillator (LO) before detection; this can be achieved using a 90° optical hybrid [15].

It mixes two input signals (an incoming signal and an optical local oscillator reference signal) and generates four optical signals with a 90-degree phase difference; by adding two pairs of balanced photodiodes, it recovers the relative phase information between the input signals. In Figure 1.15 is represented its operational scheme [16].

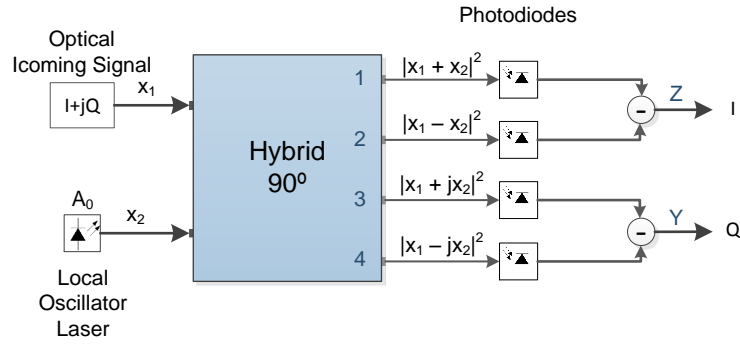


Figure 1.15 Hybrid 90° Scheme

There are four outputs each of them going to a photodiode. These photodiodes will transform the optical input into the electrical domain and then by subtracting in pairs the output signals, it is able to amplify, recover and separate the inphase and quadrature components of the initial signal.

The following equations (1.15) and (1.16) describe the hybrid 90° basic operations. Z and Y express the amplification and recovery of the fundamental signal components I and Q respectively.

$$|x_1 + x_2|^2 = |I + jQ + A_0|^2 = (I + A_0)^2 + Q^2$$

$$|x_1 - x_2|^2 = |I + jQ - A_0|^2 = (I - A_0)^2 + Q^2$$

$$\boxed{Z = (I + A_0)^2 + Q^2 - [(I - A_0)^2 + Q^2] = 4 \cdot A_0 \cdot I} \quad (1.15)$$

$$|x_1 + jx_2|^2 = |I + jQ + jA_0|^2 = I^2 + (Q + A_0)^2$$

$$|x_1 - jx_2|^2 = |I + jQ - jA_0|^2 = I^2 + (Q - A_0)^2$$

$$\boxed{Y = I^2 + (Q + A_0)^2 - [I^2 + (Q - A_0)^2] = 4 \cdot A_0 \cdot Q} \quad (1.16)$$

Chapter 2. OFDM for Optical Networks

The main goal of this master thesis is the introduction of a new type of modulation for optical networks based on ***predistortion***. This predistortion is applied to the OFDM electrical signal in order to counteract the effect that would produce the external modulation so as to achieve a perfect amplitude modulation.

Research starts by identifying the desired output signal of a Dual Drive-MZM (DD-MZM) and then obtaining its two required inputs expressions. When solving the equations two cases are considered, the ideal for infinite value of ER and the real one, with a finite ER. All about the development and solution of the predistortion technique is explained in section 2.1.1.2.

Then the objective is to be able to work with an **oIQ transmitter plus predistortion** with the advantage, over the **conventional oIQ**, of reducing from two to one the number of external modulators and improving the resilience to lower values of ER.

First this new type of transmitter (considering the ideal and real case) has to be joined with different optical receivers so as to be tested and obtain different feasible systems. The receivers used in the simulations were ***Direct Detection*** (section 2.1.2.1), ***Basic Coherent Detection and Hybrid 90° Coherent Detection*** (both explained in section 2.1.2.2). With the result that each of the six systems worked properly as described in section Chapter 4.

Both oIQ receiver schemes considered use null-biased MZMs and thus lack the required optical carrier for DD. When using a DD receiver then, modified oIQ transmitters (both for the predistortion oIQ and for the conventional oIQ) that incorporates the Single Side Band (SSB) modulation of an electrical pure tone in order to add the required subcarrier at a convenient guardband spectral distance from the signal, will be designed and used for the performance tests.

Our proposal is for these 6 systems to be used in an OFDMA PON network so in section 2.2 classifies each of the systems according to their suitability in upstream and downstream.

2.1 Optical OFDM Systems

There exist several types of optical systems and types of classifying them. Figure 2.1 shows a scheme tailored to the studied systems in this thesis.

There is a total of 6 analysed and simulated systems. Their simulations and results are exposed in Chapter 4 and Chapter 5.

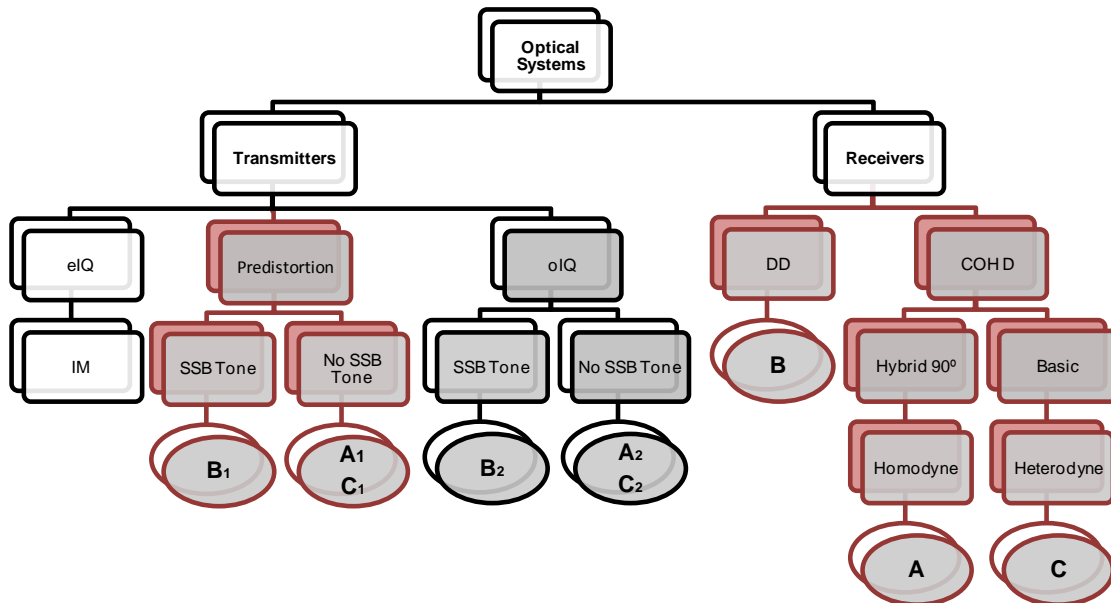


Figure 2.1 Optical Systems Classification

As seen in Figure 2.1, predistortion systems are coloured in grey and garnet in order to highlight the main important systems inside the project. Moreover conventional oIQ systems are coloured just in grey to remark them but just as comparing systems. The end of the tree finishes with circles, inside the circles there are some letters aiding to organize the systems in Chapter 4 and Chapter 5.

2.1.1 Transmitter

In this section the 4 basic types of RTO conversion module considered are described, namely conventional oIQ with and without SSB tone addition for DD, and the predistortion oIQ with and without SSB tone addition. The external MZM modulator will be the basic device in the 4 RTO converters.

2.1.1.1 Conventional oIQ

The figure shows the basic scheme of the oIQ. As seen, it is composed of two nested MZMs in a second Mach Zehnder interferometer in which the relative phase between the branches is 90° .

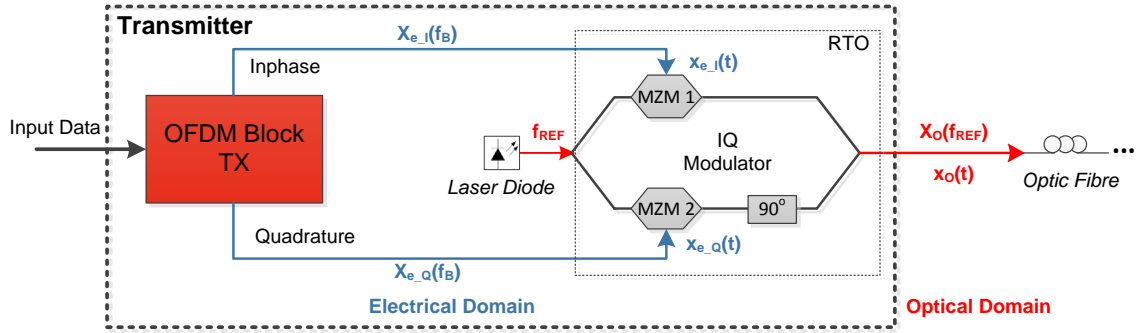


Figure 2.2 oIQ OFDM Transmitter

Since the two MZM are biased at the null point, the modulated optical signal amplitude into each branch is proportional to the driving voltage applied to it.

Considering $x_{e_I}(t)$ and $x_{e_Q}(t)$ as the baseband electrical OFDM real and imaginary signals respectively, $x_o(t)$ can be expressed as (2.1):

$$x_o(t) = e^{j(w_{LD}t + \phi_{LD})} \cdot x_{e_I}(t) + e^{j(w_{LD}t + \phi_{LD} + 90^\circ)} \cdot x_{e_Q}(t) \quad (2.1)$$

Where w_{LD} and ϕ_{LD} are the angular frequency and phase of the optical carrier generated by the laser diode [1].

In relation to operation of this device it is important to note that it requires careful adjustment of a total of 3 DC biases, one for maintaining each of the MZMs into their null point and another for the pi additional phase shift between branches. Due to the complex nature of the integrated circuit required another technological challenge featuring a trade-off between performance and cost, is to ensure high enough ER in each of the nested interferometers.

2.1.1.2 Predistortion

This type of modulation's technique aims to improve some of the restrictions of the conventional oIQ systems as well as to reduce the final cost of the transmitter's implementation.

The idea is to obtain an equivalent oIQ modulator by making use of predistortion circuits over a simpler optical modulator device structure, so to overcome the drawbacks observed in the operation of conventional oIQs.

The simple proposal of this work is to use a dual-drive MZM in which each interferometric branch is driven by a signal obtained from the real and imaginary parts of the OFDM signal through a mathematical predistortion function so that the resulting optical signal after modulation is the optical IQ combination of the real and imaginary parts of the OFDM signal (see Figure 2.5).

The two DD-MZM driving functions named $f(I,Q)$ and $g(I,Q)$ have as their inputs the Inphase and Quadrature signal components. The functions will depend on other different parameters but the most important will be γ , explained in MZM definition in section 1.2.2.4.

As γ is related to ER the fact of being able to compensate a reduced ER of a low cost MZM through digital preprocessing is also an interesting feature of the predistortion technique.

In order to solve the problem of finding the predistortion functions there have been taken into account the two possible solutions, considering $\gamma = 1$ (ideal case) and $\gamma \neq 1$ (real case).

So as to understand the expression for obtaining the resulting functions it has to be analysed the system itself, shown in Figure 2.3.

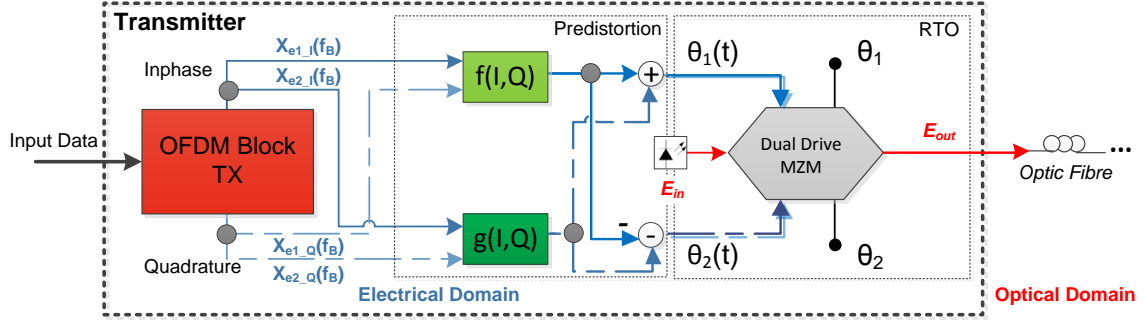


Figure 2.3 Predistortion's Scheme with a DD-MZM

The starting expression to obtain both functions is the output signal of the MZM, E_{out} :

$$E_{out} = E_{in} \cdot H_{DD_MZ}(t) = E_{in} \cdot [e^{j\theta_1} \cdot e^{j\theta_1(t)} + \gamma \cdot e^{j\theta_2} \cdot e^{j\theta_2(t)}]; \quad (2.2)$$

Then,

$$E_{out} = E_{in} \cdot e^{j\theta_1} \cdot [e^{j\theta_1(t)} + \gamma \cdot e^{j(\theta_2 - \theta_1)} \cdot e^{j\theta_2(t)}]; \quad (2.3)$$

When $[\Delta\theta_B = \theta_2 - \theta_1]$:

$$E_{out} = E_{in} \cdot e^{j\theta_1} \cdot e^{j\left(\frac{\theta_1(t) + \theta_2(t)}{2}\right)} \cdot \left[e^{j\left(\frac{\theta_1(t) - \theta_2(t)}{2}\right)} + \gamma \cdot e^{j(\Delta\theta_B)} \cdot e^{j\left(\frac{\theta_2(t) - \theta_1(t)}{2}\right)} \right]; \quad (2.4)$$

➤ **Case 1** → $\boxed{\gamma = 1 \ \& \ \Delta\theta_B = 0}$

In the following expression $E_{in} \cdot e^{j\theta_1}$ is named as C and it is a constant.

$$\begin{aligned} E_{out} &= C \cdot e^{j\left(\frac{\theta_1(t) + \theta_2(t)}{2}\right)} \cdot 2 \cdot \left[\frac{e^{j\left(\frac{\theta_1(t) - \theta_2(t)}{2}\right)} + e^{j\left(\frac{\theta_2(t) - \theta_1(t)}{2}\right)}}{2} \right] = \\ &= C \cdot 2 \cdot \cos\left(\frac{\theta_1(t) - \theta_2(t)}{2}\right) \cdot e^{j\left(\frac{\theta_1(t) + \theta_2(t)}{2}\right)} = I + jQ; \end{aligned} \quad (2.5)$$

Now the module and the phase will be obtained (constants are not considered):

From the Module:

$$|E_{out}| = 2 \cdot \cos\left(\frac{\theta_1(t) - \theta_2(t)}{2}\right) = \sqrt{I^2 + Q^2}; \quad (2.6)$$

$$\theta_1(t) - \theta_2(t) = 2 \cdot \cos^{-1}\left(\frac{\sqrt{I^2 + Q^2}}{2}\right); \quad (2.7)$$

From the Phase:

$$\varphi_{E_{out}} = \left(\frac{\theta_1(t) + \theta_2(t)}{2}\right) = \tan^{-1}\left(\frac{Q}{I}\right); \quad (2.8)$$

$$\theta_1(t) + \theta_2(t) = 2 \cdot \tan^{-1}\left(\frac{Q}{I}\right); \quad (2.9)$$

From the above the MZM branches driving functions $\theta_1(t)$ and $\theta_2(t)$ are obtained:

$$\theta_1(t) = \cos^{-1}\left(\frac{\sqrt{I^2+Q^2}}{2}\right) + \tan^{-1}\left(\frac{Q}{I}\right) \quad (2.10)$$

$$\theta_2(t) = \tan^{-1}\left(\frac{Q}{I}\right) - \cos^{-1}\left(\frac{\sqrt{I^2+Q^2}}{2}\right) \quad (2.11)$$

When looking back on Figure 2.3 is easy to extract both sought functions:

$$f(I, Q) = \frac{\Delta\theta(t)}{2} = \cos^{-1}\left(\frac{\sqrt{I^2+Q^2}}{2}\right) \quad (2.12)$$

$$g(I, Q) = \frac{\Sigma\theta(t)}{2} = \tan^{-1}\left(\frac{Q}{I}\right) \quad (2.13)$$

According to the derivation, these functions in the scheme of Figure 2.5 should allow to obtain an oIQ signal with MZM and $\gamma = 1$, resulting in MZM with very high ER. The results shown in sections 4.1 and 4.3 using an ER=120 dB confirm the correct operation and the comparison with conventional oIQ in different setups.

In order to test the ability of the predistortion technique to overcome limitations in the optical devices, such as a limited ER, following we derive extended f and g mathematical expressions valid for any value of gamma. The above expressions should then be a particular case obtained when setting $\gamma = 1$ in the generalized expressions of the next section.

➤ **Case 2** → $\gamma \neq 1$ & $\Delta\theta_B = 0$

Starting from equation (2.3) and ignoring the constants the following solutions are obtained:

$$E_{out} = \cos(\theta_1(t)) + j \cdot \sin(\theta_1(t)) + \gamma \cdot [\cos(\theta_2(t)) + j \cdot \sin(\theta_2(t))]; \quad (2.14)$$

From the Module:

$$|E_{out}| = \sqrt{[\cos(\theta_1(t)) + \gamma \cdot \cos(\theta_2(t))]^2 + [\sin(\theta_1(t)) + \gamma \cdot \sin(\theta_2(t))]^2}; \quad (2.15)$$

By multiplying and reducing the expression with the basic trigonometric equation

$$1 = \cos^2 x + \sin^2 x \quad (2.16)$$

And converting the product in a sum in the following expression is obtained (as before it will be equal to the absolute value of I and Q):

$$|E_{out}| = \sqrt{1 + \gamma^2 + 2 \cdot \gamma \cdot \cos(\theta_1(t) - \theta_2(t))} = \sqrt{I^2 + Q^2} \quad (2.17)$$

Obtaining the difference between phases $\theta_1(t)$ and $\theta_2(t)$:

$$\theta_1(t) - \theta_2(t) = \cos^{-1}\left(\frac{I^2+Q^2-1-\gamma^2}{2 \cdot \gamma}\right) \quad (2.18)$$

From the Phase:

Starting from equation (2.4) and considering $\cos(-x) = \cos x$ & $\sin(-x) = -\sin x$, it is obtained:

$$E_{out} = C \cdot e^{j\left(\frac{\theta_1(t)+\theta_2(t)}{2}\right)} \cdot \left[\cos\left(\frac{\theta_1(t)-\theta_2(t)}{2}\right) \cdot (1 + \gamma) + j \cdot \sin\left(\frac{\theta_1(t)-\theta_2(t)}{2}\right) \cdot (1 - \gamma) \right]; \quad (2.19)$$

Then E_{out} 's phase is gotten as follows:

$$\varphi_{E_{out}} = \frac{\theta_1(t) + \theta_2(t)}{2} + \left(\tan^{-1} \left[\frac{1-\gamma}{1+\gamma} \cdot \tan \left(\frac{\theta_1(t) - \theta_2(t)}{2} \right) \right] \right) = \tan^{-1} \left(\frac{Q}{I} \right); \quad (2.17)$$

Now $\theta_1(t) - \theta_2(t)$ is substituted by the expression (2.18) and by arranging the equation both phases yield:

$$\theta_1(t) = \frac{\Sigma\theta(t) + \Delta\theta(t)}{2} = \frac{1}{2} \cdot \left[2 \cdot \tan^{-1} \left(\frac{Q}{I} \right) - \tan^{-1} \left(\frac{1-\gamma}{1+\gamma} \cdot \tan \left(\frac{1}{2} \cdot \cos^{-1} \left(\frac{I^2 + Q^2 - 1 - \gamma^2}{2 \cdot \gamma} \right) \right) \right) + \cos^{-1} \left(\frac{I^2 + Q^2 - 1 - \gamma^2}{2 \cdot \gamma} \right) \right]; \quad (2.18)$$

$$\theta_2(t) = \frac{\Sigma\theta(t) - \Delta\theta(t)}{2} = \frac{1}{2} \cdot \left[2 \cdot \tan^{-1} \left(\frac{Q}{I} \right) - \tan^{-1} \left(\frac{1-\gamma}{1+\gamma} \cdot \tan \left(\frac{1}{2} \cdot \cos^{-1} \left(\frac{I^2 + Q^2 - 1 - \gamma^2}{2 \cdot \gamma} \right) \right) \right) - \cos^{-1} \left(\frac{I^2 + Q^2 - 1 - \gamma^2}{2 \cdot \gamma} \right) \right]; \quad (2.19)$$

And again the sought functions or the functions that would be introduced in real predistortion systems are the following:

$$f(I, Q) = \frac{\Delta\theta(t)}{2} = \frac{\cos^{-1} \left(\frac{I^2 + Q^2 - 1 - \gamma^2}{2 \cdot \gamma} \right)}{2} \quad (2.20)$$

$$g(I, Q) = \frac{\Sigma\theta(t)}{2} = 2 \cdot \tan^{-1} \left(\frac{Q}{I} \right) - \tan^{-1} \frac{1-\gamma}{1+\gamma} \cdot \left[\tan \left(\frac{1}{2} \cdot \cos^{-1} \left(\frac{I^2 + Q^2 - 1 - \gamma^2}{2 \cdot \gamma} \right) \right) \right] \quad (2.21)$$

Following expression (found it as well in section 1.2.2.4) represents the relation in linear scale of ER and γ :

$$ER = \left(\frac{1+\gamma}{1-\gamma} \right)^2 \quad (2.22)$$

Initially, when first real predistortion system were implemented into the VPI (software tool) and simulated we obtained dissatisfactory results. After looking over the whole system searching for the failure we discovered VPI was using another expression to associate these two parameters (in logarithmic scale):

$$ER (dB) = 10 \cdot \log \frac{\gamma^2 + 1}{\left(\frac{1-\gamma^2}{2} \right)^2} \quad (2.23)$$

Therefore in order to get a proper behaviour of real predistortion systems, the inverse function of (2.23) had to be introduced into the software's script:

$$\gamma = \pm \sqrt{\frac{2+ER \pm \sqrt{6 \cdot ER + 4}}{ER}} \quad (2.24)$$

The reason of adding this expression is to be able to compensate the ER , being an external parameter fixed by the user.

2.1.1.3 Single Side Band Tone Generation

SSB tone generation technique is used to add an electrical tone for generating an optical carrier required for DD.

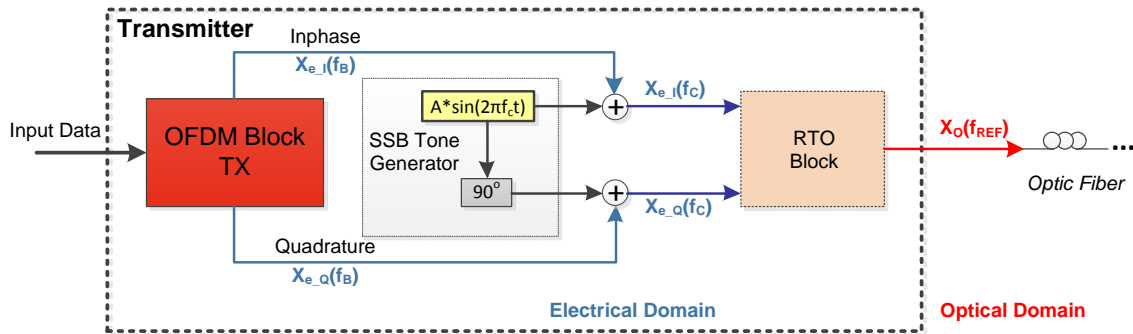


Figure 2.4 oIQ with SSB Tone

In Figure 2.4 is seen this module is embedded in the transmitter side where a sinus and a cosine are generated. The considered frequency in the simulations is the same as for auxiliary carriers in the receiver side, this is $f_c=15\text{GHz}$.

2.1.2 OFDM Receiver

In this thesis three types of receivers will be used to simulate the different optical systems: *Direct Detection* receiver (*DD*), section 2.1.2.1, *Basic and conventional Coherent Detection* receiver (*COH D*), section 2.1.2.2.

All receivers use photodiodes (section 1.2.2.3) to convert the incoming signal from optical domain to electrical one although each system has its own structure, as it will be seen below. The main difference between *DD* and *COH D* is the introduction of an optical auxiliary carrier at the beginning of the *COH D*'s photodiode or *OTR* module, working as a local oscillator, therefore having into account its phase coherence.

When an optical signal is detected by mixing with light coming from a different laser source, phase noise degrades the detected signal so that either very expensive lasers with narrow laser linewidths or phase noise compensation techniques or both, are required. In this thesis we do not aim at tackling these problems and therefore very low phase linewidth and correlation among all laser sources used in the simulations have been considered.

It has to be noted all receivers' schemes will be defined with the OFDM Block since this thesis is based in an Optical OFDM system. The OFDM Block at the receiver side handles the signal's decoding and de-mapping, being the last system's step to obtain the sent data.

2.1.2.1 Direct Detection, DD

It is the most basic type of optical receiver and is normally linked with the *IM* transmitter's type (*IM/DD* system found in section 1.1.1.1). This receiver is based on a photodiode that only responds to changes in the power level (intensity) that falls directly on it. The photodetector then transform the optical power level variation back to the original signal format [14].

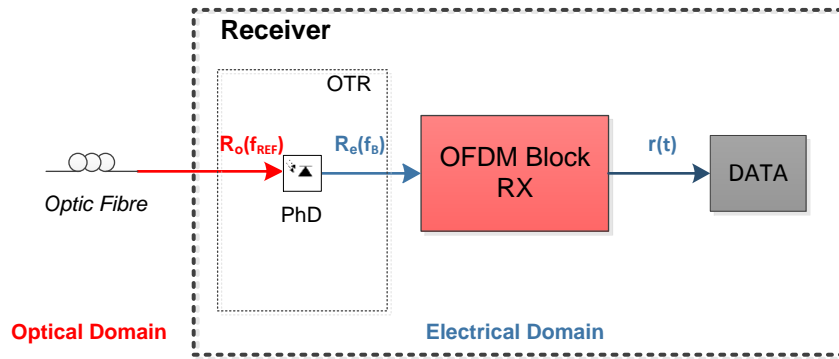


Figure 2.5 Direct Detection Receiver Scheme

As shown in Figure 2.5 the OTR module just requires a component capable of converting the optical signal into its electrical homologue. In case it is required, a down-converter module will be added in order to locate the signal in base band.

2.1.2.2 Coherent Detection, COH D

Optical communication systems using Homodyne and Heterodyne detection are called Coherent Optical Communication systems. Their implementation depends on the **phase coherence** of the optical auxiliary carrier.

Coherent Detection Techniques treat the light as a carrier medium where the information signal can be amplitude, frequency or phase modulated.

Both Heterodyne/Homodyne and basic/conventional types of coherence detection have been implemented in this thesis. They are all part of different OTR modules.

- **Basic Coherent Detection**

It comprises a laser, working as a local oscillator, and a photodiode. Following the two possible types of receivers are explained:

- **Heterodyne**

When the carrier signal frequency and local oscillator frequency are not equal is produced. This case requires down-converting the signal into baseband by adding a module between the OTR and the OFDM Block RX.

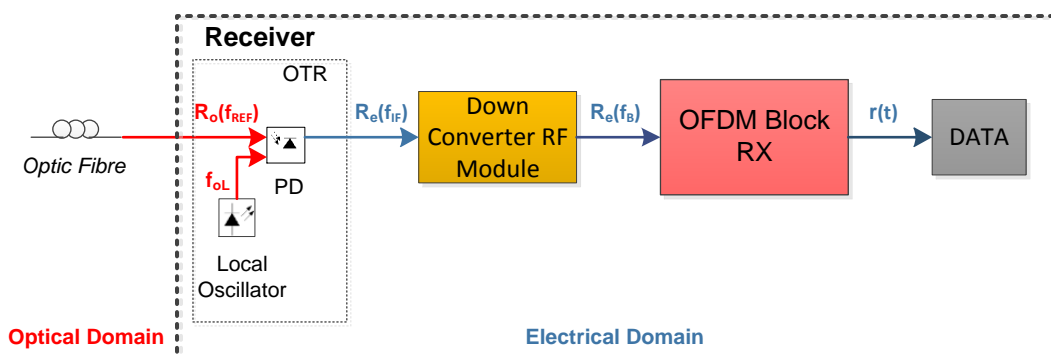


Figure 2.6 Basic Heterodyne Coherent Detection Scheme

As Figure 2.6 shows, the optical signal coming from the optic fibre $R_o(f_{ref})$, is mixed with the auxiliary carrier at f_{OL} (introduced by the local oscillator) inside the photodetector. The photodetector's output will be an electric signal located at the intermediate frequency, different to zero, therefore a bandpass signal is obtained.

In order to introduce $R_o(f_{ref})$ into the OFDM Block RX (where the baseband OFDM signal will be decoded and de-mapped as in section 1.1.1.3), the resultant signal $R_{e1}(f_{IF})$ has to be down converted to base band. That is the requirement of adding the yellow module and then obtaining the out-coming signal $R_2(f_B)$. f_B denotes the resulting signal is located in baseband and ready to be introduced in the receiver's OFDM Block.

- **Basic Homodyne Coherent Detection**

When the carrier signal frequency and local oscillator frequency are equal is produced. This results in a $f_{IF} = 0$, bringing the input signal directly to Base Band at the receiver side and so sparing the additional heterodyne module.

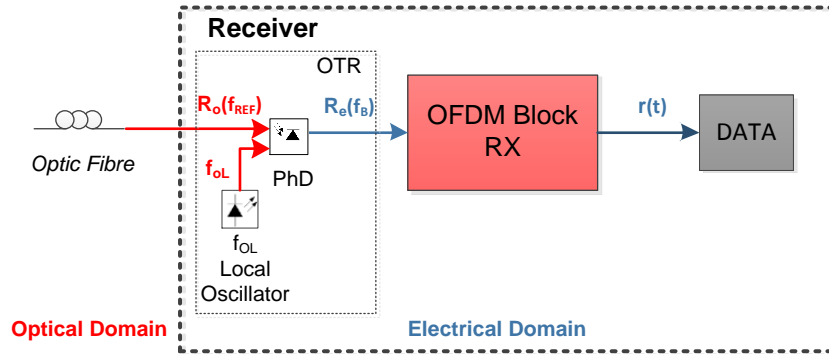


Figure 2.7 Basic Homodyne Coherent Detection Scheme

Comparing Figure 2.6 with Figure 2.7 the missing module introduced in the basic heterodyne scheme is observed. In this case when mixing the optical signal $R_o(f_{ref})$ with the auxiliary carrier at f_{OL} the resultant electrical signal $R(f_B)$ is located directly in the base band ($f_{ref}=f_{OL}$). Now $R(f_B)$ can be normally processed by the OFDM Block.

- **Conventional Coherent Detection**

The most common type of coherent detector is the one using a hybrid 90° (2×4). One of the inputs of this type of optical coupler is the received optical signal and a laser is the other. Each of the outputs goes directly to a photodetector that combining the electrical outputs results in an amplified electrical signal split in its inphase and quadrature components (more about the hybrid 90° is found in section 1.2.2.5).

As in basics coherent detection there are heterodyne and homodyne systems (Figure 2.8 and Figure 2.9). In this master thesis homodyne conventional COH D receivers have been used where $f_{OL}=f_{REF}=193.1$ THz (being f_{REF} the reference frequency of the optical fibre, section 1.2.2.2).

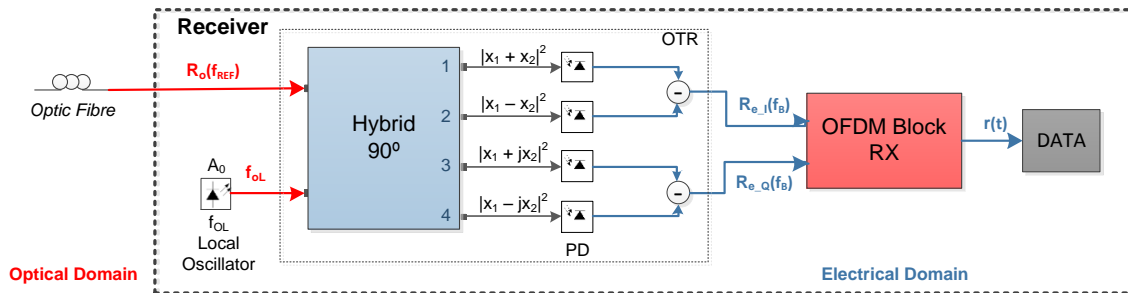


Figure 2.8 Homodyne Conventional Coherent Detection Receiver Scheme

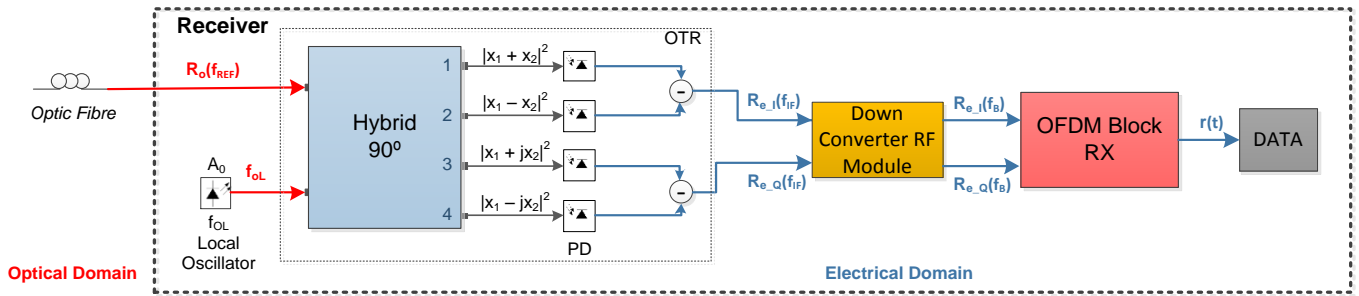


Figure 2.9 Heterodyne Conventional Coherent Detection Receiver Scheme

2.2 OFDMA PON

When speaking about OFDMA PON networks it has to be taken into account the two different edges of the communication, the users edge (ONU) and the central or switch edge (OLT).

Usually the ONU's devices will be acquired by the optical service customer and the OLT's devices will be acquired by the company deploying the network, so the price of the ONU's devices has to be affordable for the costumers. This is one of the requirements for designing the optical systems.

Therefore the different systems can be classified depending on the communication's direction. When the signal is sent from the ONU to the OLT the system's link inside the optical network is identified as the **UpStream**. When this is on the opposite direction, from the OLT to the ONU, it is identified as **DownStream** link.

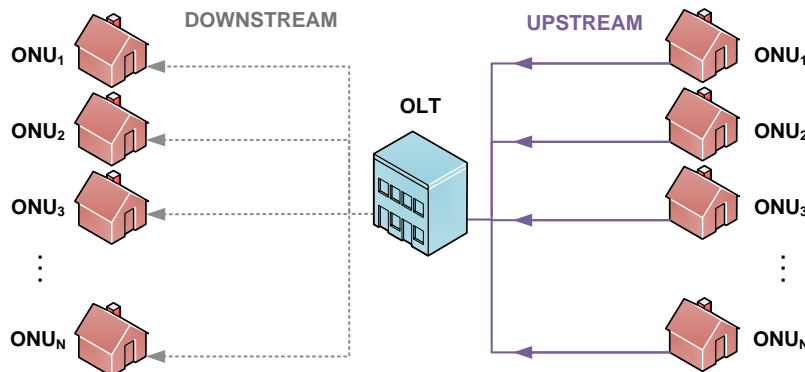


Figure 2.10 Basic PON structure scheme

As told before, when having into account the two end sides of the communication (ONU or OLT), then appropriated system for each types of links will be found. The studied systems are classified in the following list:

DOWNSTREAM	
Transmitter OLT	Receiver ONU
<ul style="list-style-type: none"> i. oIQ ii. oIQ with SSB tones generation iii. Predistortion iv. Predistortion with SSB tones generation 	<ul style="list-style-type: none"> • Direct Detection (ii and iv) • <i>Basic Coherent Detection (i andiii)</i>

Table 2.1 Downstream Systems

UPSTREAM	
Transmitter ONU	Receiver OLT

<i>i.</i> Predistortion <i>ii.</i> oIQ	<ul style="list-style-type: none"> • Basic Coherent Detection (<i>i</i> and <i>ii</i>) • Conventional Coherent Detection (<i>i</i> and <i>ii</i>)
---	---

Table 2.2 Upstream Systems

Table 2.1 and Table 2.2 show a type of receiver and a type of transmitter, respectively, coloured in grey. These types of subsystems would be too expensive for a regular customer but not so for medium or large companies working as ONUs.

In general Coherent Detection is not cheap due to the lasers and the hybrid devices involved. In order to have the lowest phase noise introduced by the lasers of the system (MZM and local oscillator lasers) they must have a very narrow linewidth value. The narrower the linewidth, the more expensive is the laser device, hence raising the prices of the subsystem making it unreachable for a regular customer.

Likewise, oIQ transmitters require the use of two external modulators or MZMs therefore increasing the subsystem's price being too expensive for a regular customer.

Each of the receivers inside the tables is related with its correspondent transmitter type, between brackets, being altogether the different optical systems studied through this master thesis.

Chapter 3. Simulations Background

This chapter introduces the software used in the different systems simulations (section 3.1) as well as a listing of the general setting parameters (section 3.3).

The other important section is the one describing the OFDM coder/decoder, 1.1.1.3. It has to be noted that the master thesis' goal has not been the design of this modules but in order to test the different 6 optical OFDM systems they have been inherited from previous works belonging to members of the same Accordance project's group.

3.1 Simulation's Tool

In order to test the theoretical systems with the purpose of getting experimental results VPIphotonics tool has been used. From the set of applications offered by VPIphotonics, three applications are important for this thesis:

a) *VPItransmissionMaker Optical Systems*

It is required to design, implement and simulate the optical systems. It has a huge data base with electrical/optical devices with typical default values and also many demos with different types of optical systems.

The interface of this software uses special naming. The **main system** or general system is called **universe**. Then each of the non-embedded modules is named as **galaxy**.

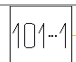
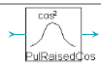

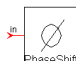
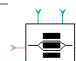
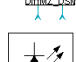
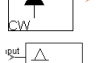

b) *VPIcomponentMaker Photonic Circuits*

It allows designing active and passive devices and abstracts their performance for simulations with a).

c) *VPIphotonicsAnalyzer*

It is a powerful data visualization and analysis tool that works with optical, electrical and numerical inputs. It is used to plot the experimental results obtained with the simulations in a)

3.1.1 Embedded Modules Used

Used Modules	Description
	<i>PRBS</i> module generates pseudo random binary sequences, PRBS.
	<i>PulseRaisedCosQAM</i> module generates a Nyquist response from an incoming electrical impulse.
	<i>FuncSineEI</i> module generates an electrical sine waveform superimposed on a constant bias.
	<i>PhaseShift</i> module applies a constant phase shift to a signal.
	<i>ModulatorDiffMZ_DSM</i> module is a generic datasheet model representation of a typical split (upper and lower) and dual (separate DC and RF) electrode configured differential Mach-Zehnder external modulator.
	<i>LaserCW</i> module models a DFB laser producing a continuous wave (CW) optical signal. If the different lasers of the system have the same seed, they are correlated.
	<i>LogicAddChannel</i> module provides the ability to "assign" logical channels stored in a global list to the signal.
	<i>UniversalFiberFwd</i> module is a simplified version of the Universal fiber module for simulation of wideband nonlinear signal transmission in optical fibers

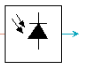
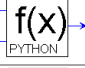
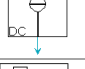
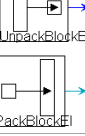
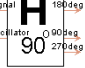
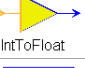


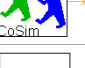






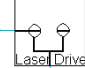

	<i>Photodiode</i> module represents a model of PIN and APD photodiodes. These can be simulated on base of predefined responsivity, avalanche multiplication, dark current and noise.
	The <i>Mathematical Expression (Python)</i> modules implement the calculation of mathematical functions of one, two, three or four variables.
	<i>DC</i> module produces a constant-amplitude electrical signal at a defined sample rate. It is used for biasing lasers or modulators.
	<i>UnpackEl</i> & <i>Pack BlockEl</i> (electric) serve as interfaces to the Signal Processing Modules.
	The <i>Hybrid90deg</i> module represents a generic 2x4 quadrature optical hybrid.
	<i>IntToFloat</i> module converts an integer input to a floating-point output.
	<i>Pack_M</i> module produces a matrix with floating-point entries constructed from floating-point input values
	<i>UnPkCx_M</i> reads a complex matrix and output its elements, row by row.
	<i>CoSimInterface</i> is a cosimulation interface, driving simulation in external tools. It supports cosimulations with Matlab, Python, dynamic link libraries and COM components.
	<i>CoSimInputMxFit</i> declares a matrix floating point input port for a cosimulation module. <i>CoSimOutputMxCx</i> declares valued output port for a cosimulation module.
	<i>CxToRect</i> converts an input of type complex to real and imaginary parts on separate ports of type float
	<i>UpSample</i> is a module that upsamples by a given factor.
	<i>AmpSysEl</i> module is a system of an electrical amplifier with additive Gaussian noise source at its output.
	<i>Matrix</i> module produces a matrix with floating-points entries
	<i>Const</i> module outputs a constant signal with value given by the level parameter.
	<i>Switch</i> module switches the input signal to one of two outputs, depending on the value of the control input.
	<i>LaserDriver</i> module is used for driving modulators that requires an arbitrary current or voltage swing.

Table 3.1 VPI embedded Modules used

3.2 OFDM Modules

These modules (galaxies) were programmed in Matlab by using the Co-Simulation tool. Galaxies variables have been defined in the Universe for an easy changing of the value of the whole system's parameters.

3.2.1 OFDM Coder

In the OFDM section, 1.1.1.3, the OFDM coder is explained in greater depth. Figure 3.1 shows the OFDM coder galaxy, it is composed by different VPI blocks such as those shown in Table 3.1. The most important block is the Co-Simulator module; this is where the programmed script responsible of getting the OFDM signal is located.

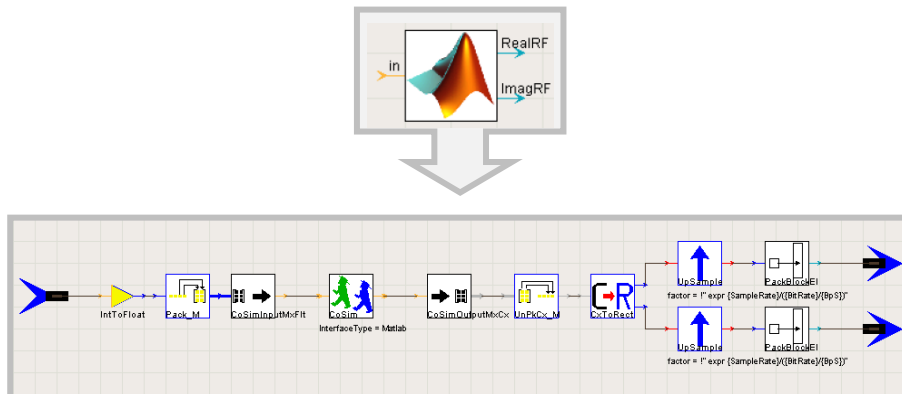


Figure 3.1 OFDM Coder Galaxy in VPI

3.2.2 OFDM Decoder

The OFDM decoder block is a more complex block since it allows reconstructing the signal that has been sent through a dispersive channel.

As shown in Figure 3.2 the decoder is composed by different blocks as a Co-simulator block, a logical channel input, a constellation block and different outputs (signal in symbols, BER, EVM and the signal in bits).

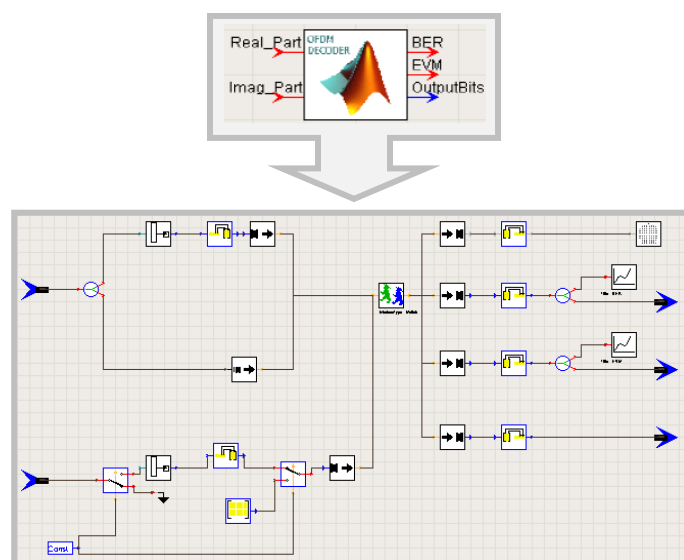


Figure 3.2 OFDM Decoder Galaxy in VPI

3.3 Universe Setting Parameters

In order to obtain correct simulation results certain conditions must be fulfilled. Figure 3.3 shows the universe setting parameters used in the simulations.

Global			
f	TimeWindow	2^{16} *(BitsPerSymbol/BitRateDefault)	s
i	GreatestPrimeFactorLimit	2	
	InBandNoiseBins	OFF	
	BoundaryConditions	Periodic	
	LogicalInformation	ON	
f	SampleModeBandwidth	1280e9	Hz
f	SampleModeCenterFrequency	193.1e12	Hz
f	SampleRateDefault	2^3 *(BitRateDefault/BitsPerSymbol)	Hz
f	BitRateDefault	10e9	bit/s
General			
f	BitsPerSymbol	2	
f	CyclicPrefix	0	
f	RollOff	0	
f	N_FFT	256	
f	Phase	90	
f	CarrierFrequency	15 *(BitRateDefault/BitsPerSymbol)	
f	A	2	
f	ER	120	
f	Vpi	1	

Figure 3.3 Universe Setting Parameters

Firstly as the input data will be modulated in a 4QAM:

$$\mathbf{BitsPerSymbol} = 2 \quad (3.1)$$

- A very important parameter to fix is the *TimeWindow*. This is the observation's period and it must comprise an integer number of bits. It is calculated as follows:

$$\mathbf{TimeWindow} = \frac{2^t \cdot \mathbf{BitsPerSymbol}}{\mathbf{BitRateDefault}} = \mathbf{131.072\mu s} \quad (3.2)$$

TimeWindow value is fixed by the total number of bits in the simulation. In our simulation a feasible result meets $BER=10^{-3}$, in order to get a significant number of errors a total of 100000 bits need to be simulated, then $t_{min} = 16$, obtaining a total of:

$$\mathbf{2^t \cdot BitsPerSymbol} = \mathbf{2^{16} \cdot 2} = \mathbf{131072\ bits} \quad (3.3)$$

- SampleRateDefault* is another influential parameter, it is defined as:

$$\mathbf{SampleRateDefault} = \frac{2^s \cdot \mathbf{BitRateDefault}}{\mathbf{BitsPerSymbol}} = \mathbf{4GHz} \quad (3.4)$$

Its numerator denotes the total number of samples, and this is:

$$\mathbf{2^s \cdot BitRateDefault} = \mathbf{8 \cdot 10^9\ Samples} \quad (3.5)$$

- BitRateDefault* parameter specifies the velocity of the transmitted bits through the system. Its value is **1 Gbps**

- *CyclicPrefix* gives the possibility of adding a cyclic prefix writing a value between 0 and 1. In the systems studied this value has been 0. It can be a future line to optimize the systems of this thesis by applying this value among other features.
- *N_FFT*: is the number of carriers available to build an OFDM signal. This parameter must be a power of two value, since represents the number of inputs of the IFFT/FFT algorithm. This value has been fixed to **256**, another future line would be testing the system with different number of carriers.
- *CarrierFrequency* is the frequency that has been used for the auxiliary carriers adding a factor of 2. In this case the *CarrierFrequency* is 7,5GHz, and in the simulation the value used is 15GHz.
- *SampleModeCentreFrequency* is the reference frequency of the fibre. And working in 3rd window this is 193.1 THz.

Chapter 4. Optical OFDM Simulated Systems

This chapter exposes the optical OFDM simulated systems being most of the chapter focused on the new proposed modulation, ***predistortion***.

Sections 4.1, 4.2 and 4.3 explain the chronological order followed to obtain a proper final assessment of ***Real Predistortion Systems***. In the development of the 3 periods, secondary systems have also been implemented: *Ideal Predistortion (1st step)* and *Conventional oIQ (3rd step)* systems. These are considered as secondary systems because they are not the master thesis's main goal but their assessments are required in order to be able to achieve it. Hence brief general descriptions of their implementation's purposes and performances are included in this chapter.

Regarding Real Predistortion Systems once their implementation process is definite, they will be renamed as simply Predistortion Systems. There is a detailed B2B system's definition in section 4.4.

4.1 Ideal Predistortion Systems in VPI – 1st Step

When expressions for ideal predistortion modulation have been obtained, (2.12) and (2.13), three different systems were implemented and tested in order to ensure a feasible performance for the master thesis' main objective, real predistortion systems (still not implemented at this step). These three predistortion systems are the same for ideal and real cases:

- ***System A₁: Predistortion & Conventional Homodyne Coherent Detection***
- ***System B₁: Predistortion plus SSB Tone & Direct Detection***
- ***System C₁: Predistortion & Basic Heterodyne Coherent Detection***

So as to implement the ideal case two python embedded modules were used, the transmitters' schemes in VPI for this case looks like Figure 4.1.

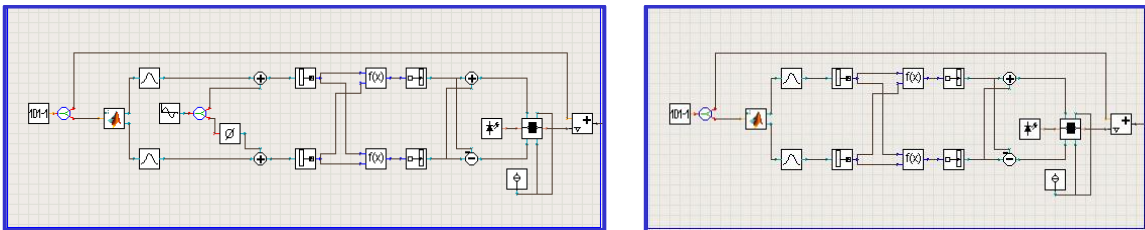


Figure 4.1 Ideal Predistortion Transmitters in VPI with and without SSB Tone generation

At the end of the systems we are able to test them by obtaining the bit error rate and their constellation diagram. These obtained diagrams for ideal transmitters with their respective receivers are shown in Figure 4.2.

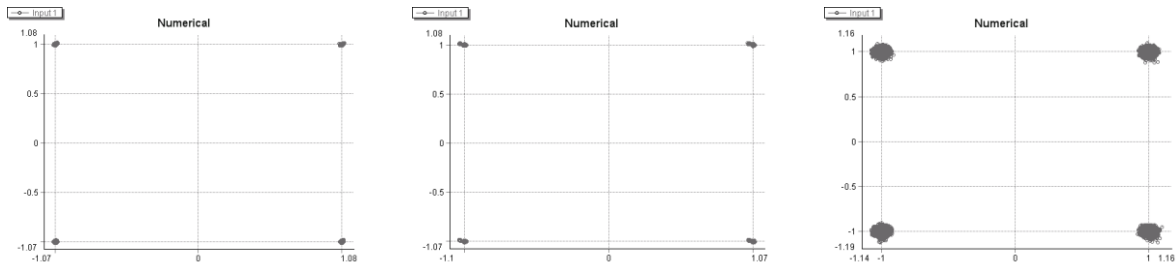


Figure 4.2 Constellation Diagram of Ideal Predistortion Systems A1, B1 and C1, respectively. With BER=0, infinite ER and fibre length not considered

Constellation diagrams tell us predistortion systems are achievable due to received symbols are allocated on or very closed to the 4QAM symbols.

After obtaining these successful results with a value of BER=0 then we followed to the next step, real predistortion systems implemented in the VPI.

4.2 Real Predistortion Systems in VPI – 2nd Step

This step starts with the implementation of the real expressions (2.20) and (2.21), first in the same python modules. When introducing the real functions into these modules they were not working properly and so a Co-simulator interface had to be used.

At the end equations (2.20) and (2.21) for the real predistortion case had to be introduced into a matlab script, running inside the Co-simulator interface. Figure 4.3 shows the galaxy for the real predistortion's systems with the different blocks in order to sample the input signal.

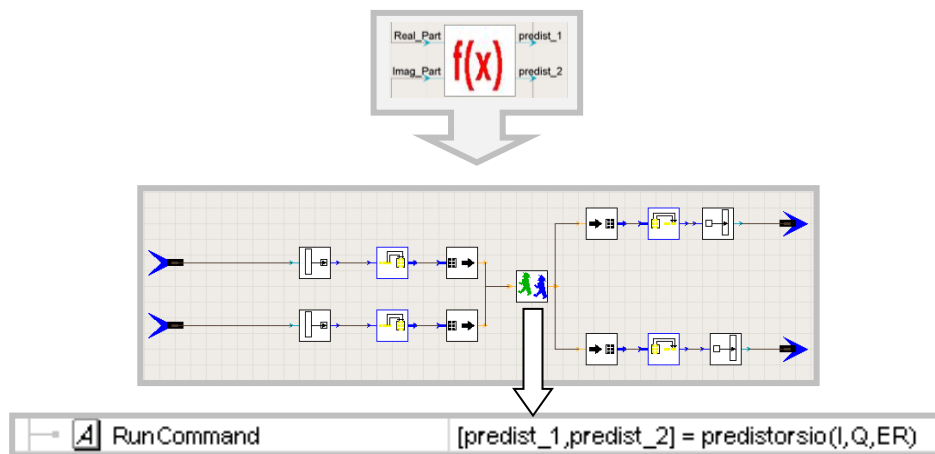


Figure 4.3 Internal Block of the Real Predistortion Module and CoSimInterface internal parameter

The three different systems schemes are detailed in section 4.4. In the same section a B2B description is found showing images of the signal at the different stages.

4.3 Conventional oIQ Systems in VPI – 3rd Step

After predistortion oIQ transmitters were proven to properly work, we aimed at comparing them in similar conditions with conventional oIQ systems (its B2B description with images at different stages is in annex C). Therefore the following step was designing and implementing in VPI the same systems but now with conventional oIQ at the transmitter side. The three implemented conventional oIQ systems with their respective representations are shown in Figure 4.4, Figure 4.5 and Figure 4.6:

➤ **System A₂: Conventional oIQ & Conventional Homodyne Coherent Detection**

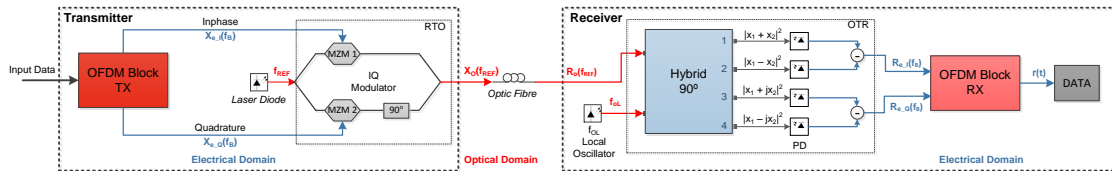


Figure 4.4 System A₂ Scheme

➤ **System B₂: Conventional oIQ plus SSB Tone & Direct Detection**

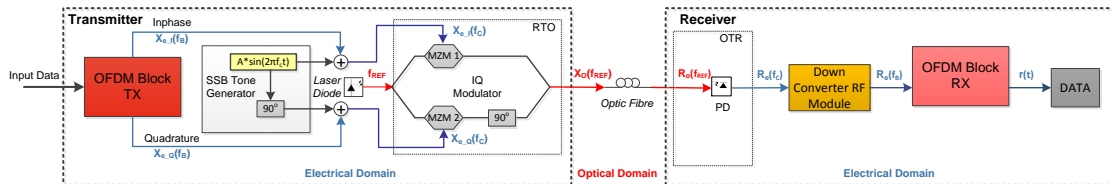


Figure 4.5 System B₂ Scheme

➤ **System C₂: Conventional oIQ & Basic Heterodyne Coherent Detection**

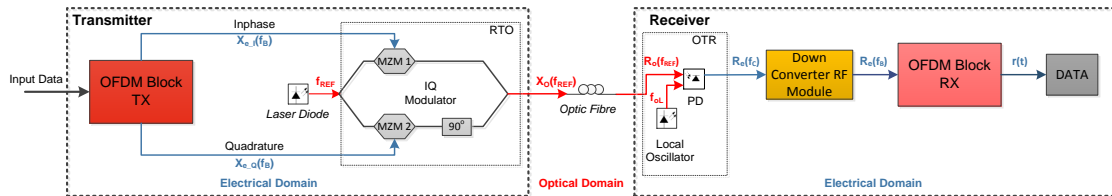


Figure 4.6 System C₂ Scheme

The transmitter side scheme implemented in VPI is shown in Figure 4.7.

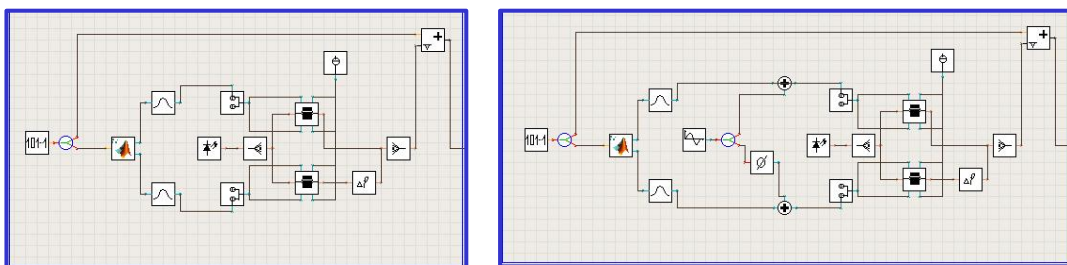


Figure 4.7 Conventional oIQ Transmitters in VPI with and without SSB Tone generation

As well as the other systems, we are able to test them by obtaining the bit error rate and their constellation diagram. These obtained diagrams for conventional oIQ transmitters with their respective receivers are shown in Figure 4.8.

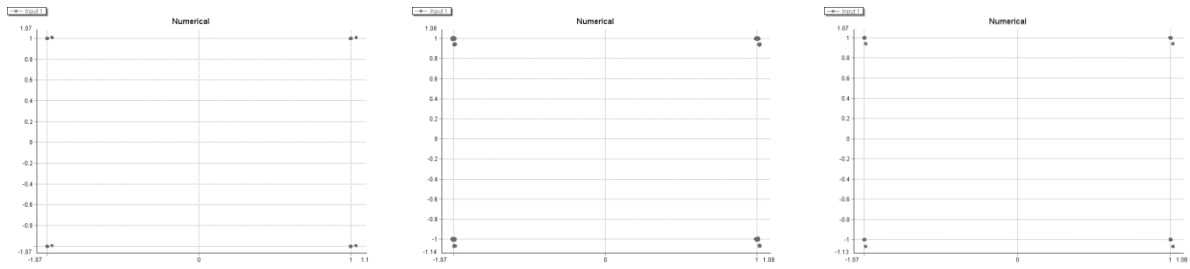


Figure 4.8 Constellation Diagram of Conventional oIQ Systems A2, B2 and C2, respectively. With BER=0, infinite ER and fibre length not considered

The results comparison with predistortion systems regarding to Sensitivity and BER versus Fibre Length and ER variation is analyzed in Chapter 5.

4.4 Predistortion Systems Description

In connection with section 4.2 this section makes a B2B description of the real predistortion systems in order to understand the different processes undergone by the input signal until its recovery. Different colours shapes have been introduced through the different system's schemes in order to visually identify the position of the graphics shown in the systems' description and in the results sections.

4.4.1 System A₁

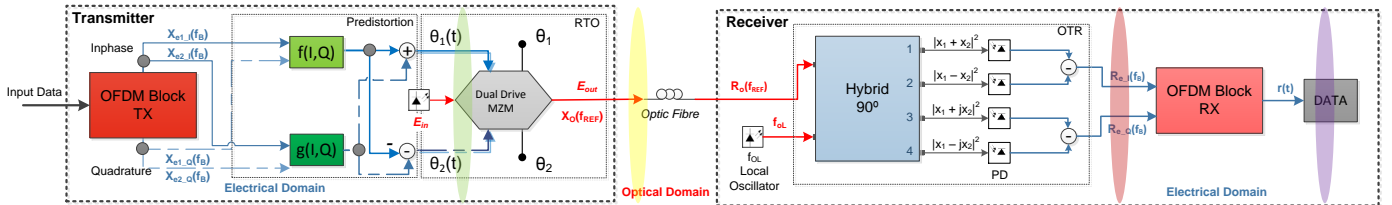


Figure 4.9 System A1 Scheme

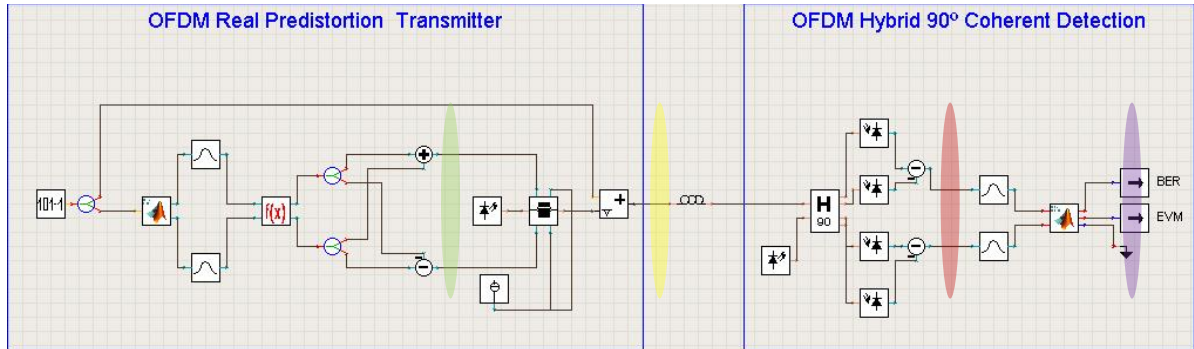


Figure 4.10 System A1 VPI's Scheme

According to Figure 4.9 and Figure 4.10 the **Input Data** is introduced into the OFDM Coder Block in order to map, modulate and encode the input signal.

The modulation used inside the OFDM Block is a 4QAM, after these symbols are encoded as an OFDM symbol (to know more about the processes of an OFDM coder, read sections 1.1.1.3 and 3.2.1).

These outputs are the electrical OFDM signal's components, each one split in two in order to be introduced in the predistortions functions, $X_{e1_I}(f_B)$, $X_{e2_I}(f_B)$, $X_{e1_Q}(f_B)$, $X_{e2_Q}(f_B)$.

Now there are four electrical signals coming from the OFDM coder block. Signals $X_{e1_I}(f_B)$ and $X_{e1_Q}(f_B)$ are injected in $f(I,Q)$; on the other hand signals $X_{e2_I}(f_B)$ and $X_{e2_Q}(f_B)$ are injected in $g(I,Q)$. The outputs of these functions have to be combined as follows:

$$\theta_1(t) = f(I, Q) + g(I, Q) \quad (4.1)$$

$$\theta_2(t) = f(I, Q) - g(I, Q) \quad (4.2)$$

Then $\theta_1(t)$ is represented in Figure 4.11 and $\theta_2(t)$ is shown in Figure 4.12.

The following step is converting $\theta_1(t)$ and $\theta_2(t)$ in an optical signal. The use of a single DD-MZM is required. Each of the functions is introduced into opposite ports of the external modulator. Moreover the optical carrier at the reference frequency of the fibre is injected too, $f_{REF} = 193.1 \text{ THz}$.

The signal coming from the RTO block is $X_o(f_{REF})$, Figure 4.13. This optical base band signal is ready to be introduced into the channel or SM optical fibre.

Once the optical signal arrives at the receiver side is introduced inside the hybrid 90° (section 1.2.2.5). This hybrid is a coupler that mixes received signal with and auxiliary carrier located at the same reference frequency due to this is a homodyne system and so the signal is located at the optical base band.

As seen in Figure 4.14 signals $R_{e_I}(f_B)$ and $R_{e_Q}(f_B)$ have been converted to base band in electrical domain with the OTR block.

Then the signal is prepared to enter inside the OFDM Decoder Block in order to recover the original sent signal (there is more information about OFDM decoder process in sections 1.1.1.3 and 3.2.2).

When analysing the constellation diagram a small phase shift is seen in the system A_1 , the distance from wrong symbols to the right ones is (0.015,-0.06). Both cases have a value of BER=0.

$ER = 120\text{dB}$ and $L=0\text{ km}$

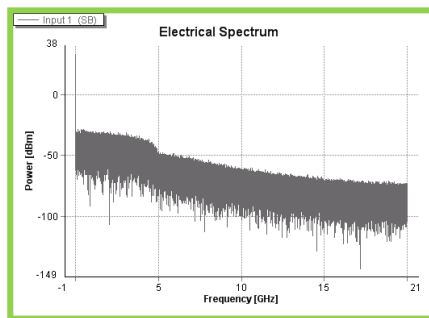


Figure 4.11 System A_1 : $\theta_1(t)$ predistortion signal

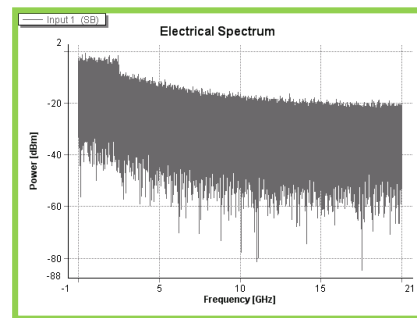


Figure 4.12 System A_1 : $\theta_2(t)$ predistortion signal

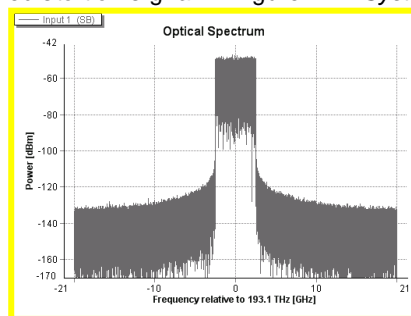


Figure 4.13 System A_1 : $X_o(f_{REF})$ with -49.38 dBm

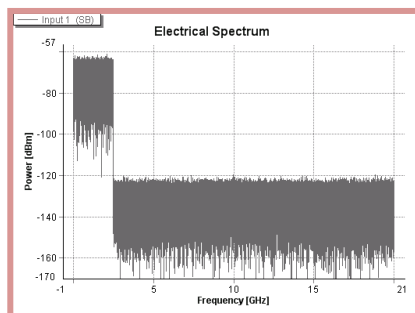


Figure 4.14 System A_1 : $R_{e_I}(f_B)$

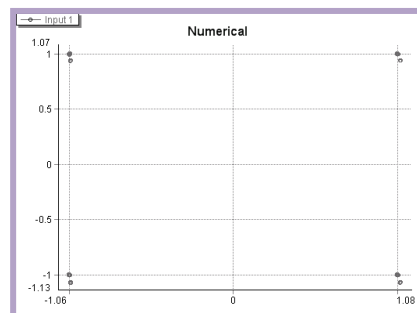


Figure 4.15 System A_1 : Constellation Diagram, BER = 0

4.4.2 System B₁

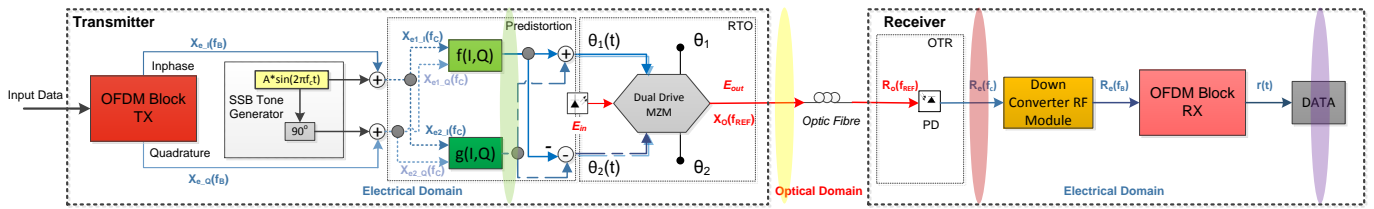


Figure 4.16 OFDM System B1 Scheme

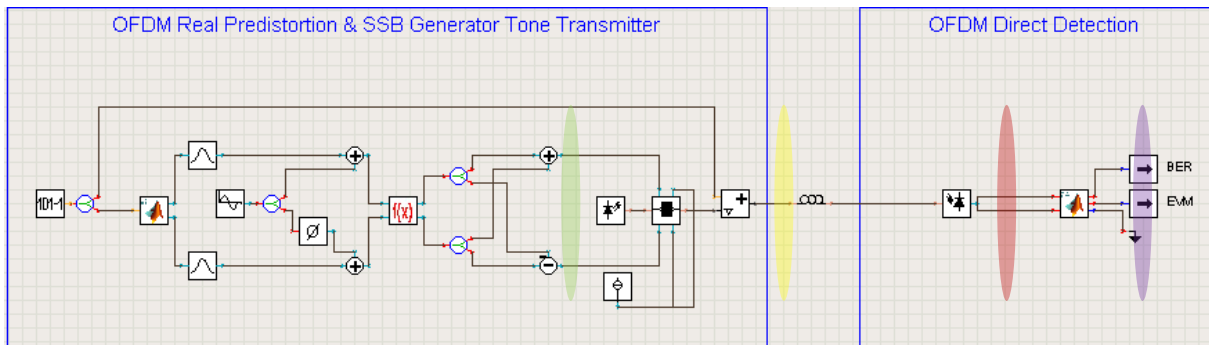


Figure 4.17 System B1 VPI's Scheme

According to Figure 4.16 and Figure 4.17 the **Input Data** is introduced into the OFDM Coder Block following the same process as in section 4.4.1.

Its outputs are the electrical OFDM signal's components $X_{e_i}(f_B)$ and $X_{e_q}(f_B)$. These signals are added to a Single Side Band tone at $f_c=15\text{GHz}$. These two signals are split into four signals in order to introduce them in the predistortion functions, so again the input to both functions are: $X_{e1_i}(f_B)$, $X_{e2_i}(f_B)$, $X_{e1_q}(f_B)$, $X_{e2_q}(f_B)$.

Again, signals $X_{e1_i}(f_B)$ and $X_{e1_q}(f_B)$ are injected in $f(I, Q)$; and $X_{e2_i}(f_B)$ and $X_{e2_q}(f_B)$ are injected in $g(I, Q)$. The outputs of these functions have to be combined as equations (4.1) and (4.2).

Now in $\theta_1(t)$ is observed how the electrical packet is shifted to 15GHz (Figure 4.18); $\theta_2(t)$ has the electrical packet located at base band but the 15GHz tones is detected, as well as some harmonics (Figure 4.19).

The following step is converting $\theta_1(t)$ and $\theta_2(t)$ in an optical signal. The use of a single DD-MZM is required. Each of the functions is introduced into opposite ports of the external modulator. Moreover the optical carrier at the reference frequency of the fibre is injected too, $f_{REF}=193.1\text{THz}$.

The process inside the DD-MZM with the predistortion technique is the same as the one explained in section 4.4.1.

The MZM's output signal is $X_o(f_{REF})$. This optical base band signal is ready to be introduced into the channel or SM optical fibre.

Now the resultant optical signal is formed by the electrical packet at the reference frequency and an optical auxiliary carrier at 15 GHz, in Figure 4.20 $X_o(f_{REF})$ is represented. This optical base band signal plus the injected auxiliary carrier are ready to be introduced into the SM optical fibre.

Once the optical signal arrives at the receiver side, $R_o(f_{REF})$, is introduced directly inside the photodiode, direct detection. This photodetector converts the optical signal into an electrical one as explained in section 1.2.2.3.

The obtained signal is an electrical side band signal located at $f_c=15\text{GHz}$, as shown in Figure 4.21. As this signal is not in base band it has to be down converter by adding an additional block as seen in Figure 4.16.

Then the signal is prepared to enter inside the OFDM Decoder Block in order to recover the original sent signal (OFDM decoder process information is in sections 1.1.1.3 and 3.2.2).

When analysing the constellation diagram a small phase shifts is seen in system B_1 , the distances from wrong symbols to the right ones is (0.025,-0.06), with a value of BER=0.

$ER = 120\text{dB}$ and $L=0\text{ km}$

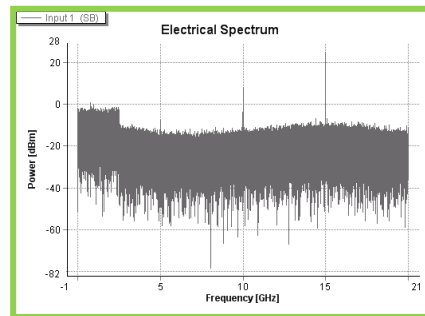
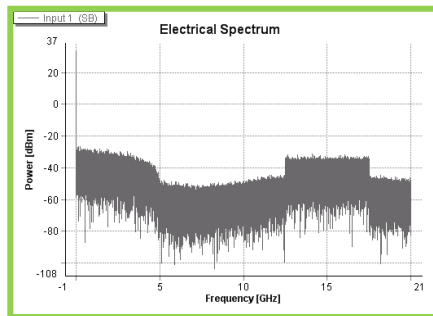


Figure 4.18 System B_1 : $\theta_1(t)$ predistortion signal Figure 4.19 System B_1 : $\theta_2(t)$ predistortion signal

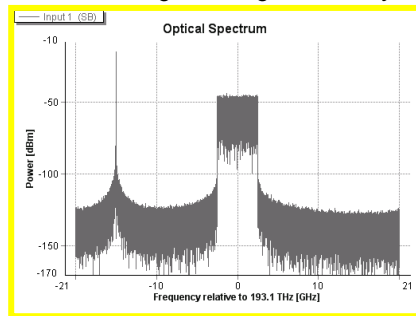


Figure 4.20 System B_1 $X_o(f_{REF})$ with -49.38 dBm plus SSB tone at 15GHz

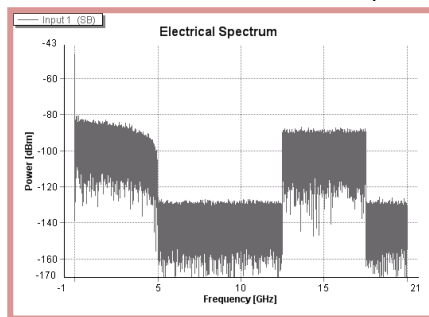


Figure 4.21 System B_1 : $R_e(f_c)$

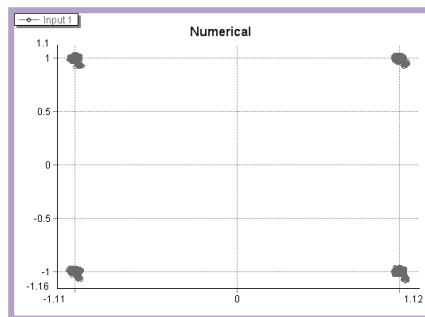


Figure 4.22 System B_1 : Constellation Diagram, BER=0

4.4.3 System C₁

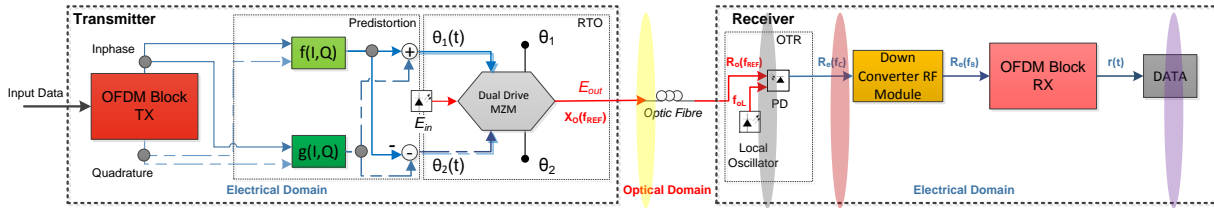


Figure 4.23 System C1 Scheme

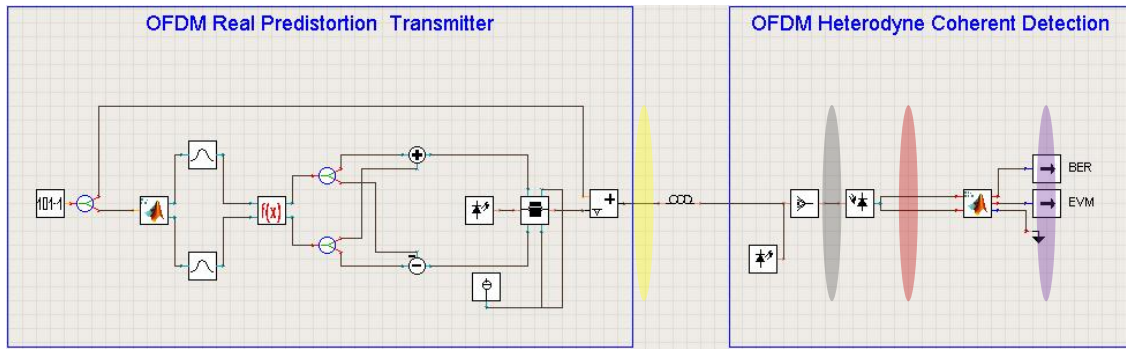


Figure 4.24 System C1 in VPI's Scheme (I)

According to Figure 4.23 and Figure 4.24 the **Input Data** is introduced into the OFDM Coder Block following the same process as in section 4.4.1. Its outputs are the electrical OFDM signal's components $X_{e1_I}(f_B)$, $X_{e2_I}(f_B)$, $X_{e1_Q}(f_B)$, $X_{e2_Q}(f_B)$.

Now there are four electrical signals coming from the OFDM coder block. Signals $X_{e1_I}(f_B)$ and $X_{e1_Q}(f_B)$ are injected in $f(l,Q)$; on the other hand signals $X_{e2_I}(f_B)$ and $X_{e2_Q}(f_B)$ are injected in $g(l,Q)$. The outputs of these functions have to be combined as equations (4.1) and (4.2).

The next step is converting $\theta_1(t)$ and $\theta_2(t)$ in an optical signal. Now is required the use of a DD-MZM. Each of the functions is introduced into opposite ports of the external modulator. Moreover the optical carrier at the reference frequency of the fibre is injected too, $f_{REF}= 193.1 THz$.

The process inside the DD-MZM with the predistortion technique is the same as the one explained in section 4.4.1.

The signal coming from the RTO block is $X_o(f_{REF})$, Figure 4.25. This optical base band signal is ready to be introduced into the channel or SM optical fibre.

Once the optical signal arrives at the receiver side is introduced into a photodiode together with an auxiliary carrier or local oscillator generating lorentzian signal at $f_c=15GHz$, Figure 4.26. This auxiliary carrier addition produces a frequency shift into the resultant electrical signal, $R_e(f_c)$, moving the received electrical packet to 15GHz, Figure 4.27.

In order to introduce $R_e(f_c)$ into the OFDM Decoder Block, it has to be down-converted to base band with the module in Figure 4.23.

Then the signal is prepared to enter inside the OFDM Decoder Block in order to recover the original sent signal (OFDM decoder process information is in sections 1.1.1.3 and 3.2.2).

When analysing the constellation diagram a small phase shift is seen in this system, the distance from wrong symbols to the right ones is (0.01,-0.06), with a value of BER=0.

$ER = 120\text{dB}$ and $L=0\text{ km}$

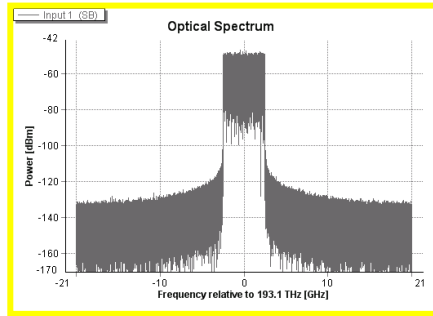


Figure 4.25 System C_1 : $X_o(f_{REF})$

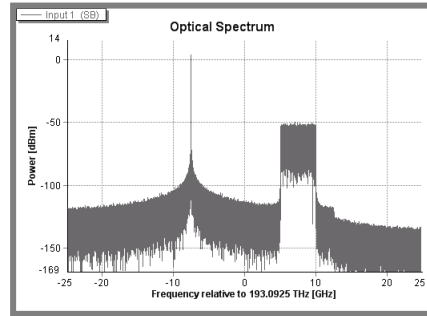


Figure 4.26 System C_1 : $X_o(f_{REF})$ plus the auxiliary carrier at 15 GHz from $X_o(f_{REF})$

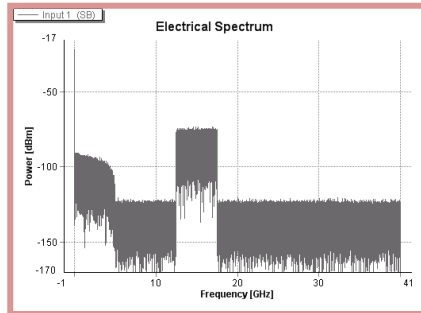


Figure 4.27 System C_1 : $R_{e_l}(f_B)$

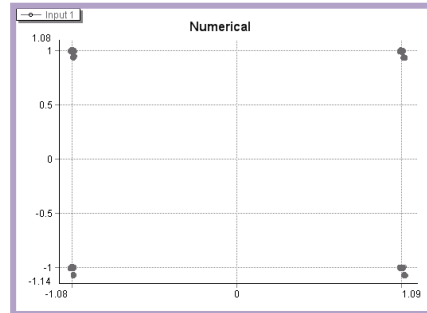


Figure 4.28 System C_1 : Constellation Diagram, BER=0

Chapter 5. Summary of Results

This chapter is organized in two sections, section 5.1 shows the results obtained from the conventional oIQ and predistortion systems regarding to sensitivity levels versus fibre length. Section 5.2 is devoted to analyze different results regarding to ER variation in the simulated systems.

5.1 Sensitivity versus Fibre Length

VPI allows the design of iterative simulation procedures in which successive simulations can be programmed with changing settings by means of a TCL programming language. For the results in this section a TCL code was written in order to find the minimum received power required for a $BER=10^{-3}$. The algorithm consisted on changing in steps the attenuation introduced prior to reception until the BER value was in a reduced margin around 10^{-3} . The steps and the margin value were chosen to meet a trade-off between accuracy of the results and simulation time. The script is found in annex D.

The results show that performance of conventional oIQ and predistortion systems, when extracting the systems' sensitivity versus the fibre length, are very similar to each other when considering a high ER. Comparing the first and most constant sensitivity value of the three different systems (regarding to different receivers), systems B₁&B₂ require a very high value of $S_B=-23 \text{ dBm}$ (Figure 5.2) while in systems A₁&A₂ and C₁&C₂ these values are around $S_A=-50 \text{ dBm}$ and $S_C=-47.5 \text{ dBm}$ respectively (Figure 5.1).

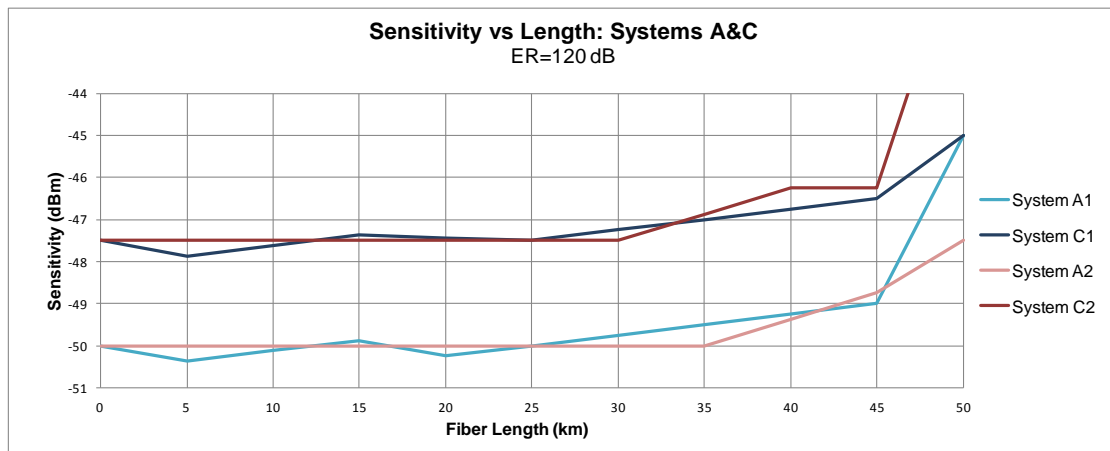


Figure 5.1 Sensitivity vs Length Systems A1, C1, A2, and C2

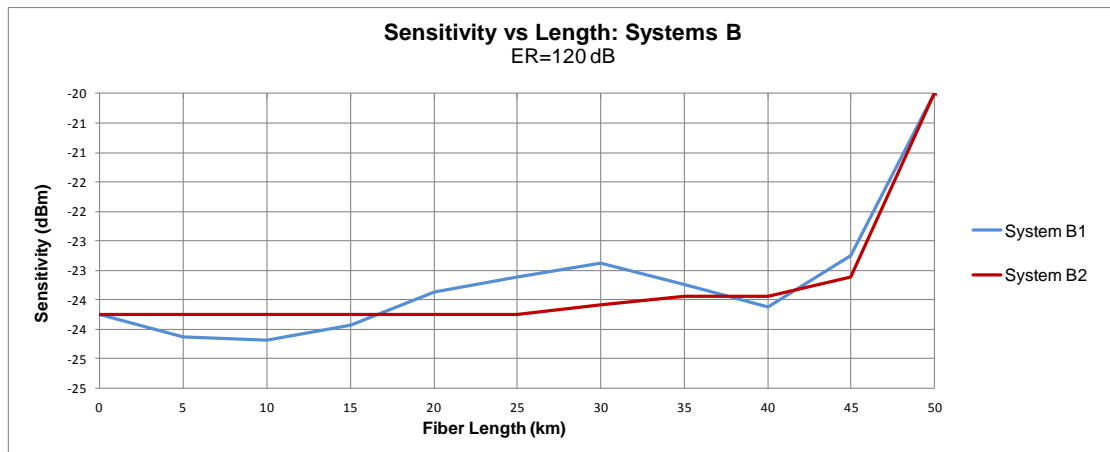


Figure 5.2 Sensitivity vs Length Systems B1 and B2

On the other hand all systems have in common that from 45km the required sensitivity increases sharply. Also when $L=45\text{km}$ there is a 1 dB increment from the last sensitivity value obtained.

5.2 ER variation

When testing the conventional oIQ systems with a low ER value, we found that for example with $ER=30\text{dB}$ they are no longer feasible systems due to its $BER=0.00188$. In Figure 5.3 the constellations of the three conventional oIQ systems are shown, a wrong system performance is found when a replica constellation appears far away from the original.

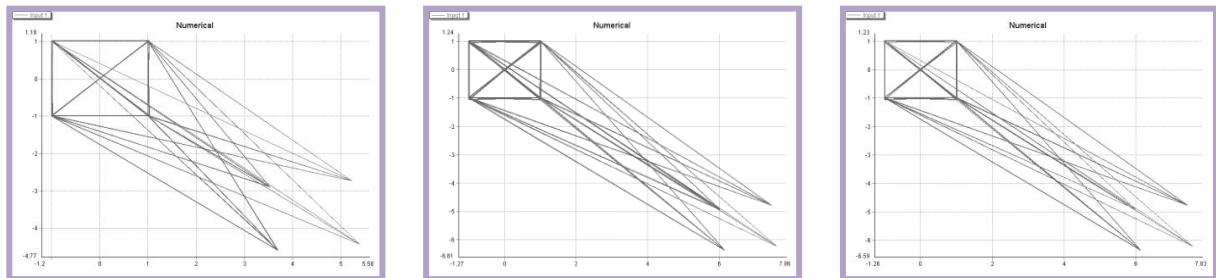


Figure 5.3 Constellation Diagram of Conventional oIQ Systems A2, B2 and C2, respectively.
With $BER=0.00188$, $ER=30$ and fibre length not considered

This ER value has been fixed as well in predistortion systems resulting in a proper behaviour of the three systems; in general predistortion systems are more resilient to lower ER values

In Figure 5.4 systems A_1 and C_1 symbols have been spread out but they are still around the correct area of the 4QAM modulation. Regarding to system B_1 a small chirp effect is observed but it is still a correct result. Apart from those detected effects all 3 systems have still a $BER=0$.

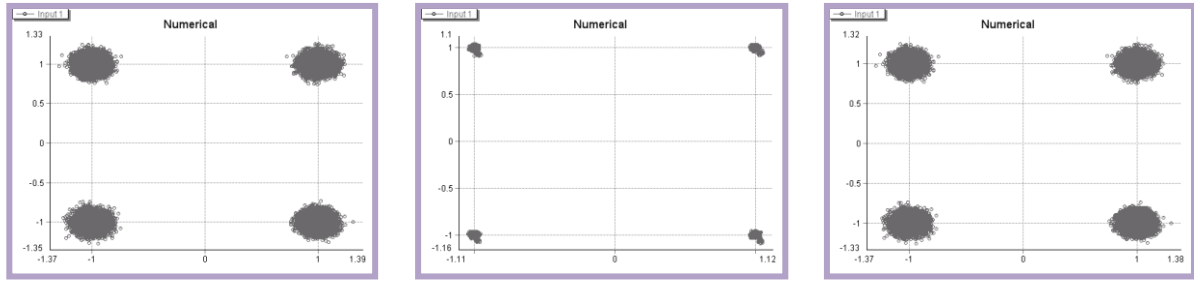


Figure 5.4 Constellation Diagram of Real Systems A1, B1 and C1, respectively. With BER=0, ER=30 and fibre length not considered

Likewise predistortion systems have been tested in order to obtain results in terms of BER versus ER (using B2B systems). Measurements have been done from $ER_{min}=7dB$ until getting a BER=0 and with $L=0$ km.

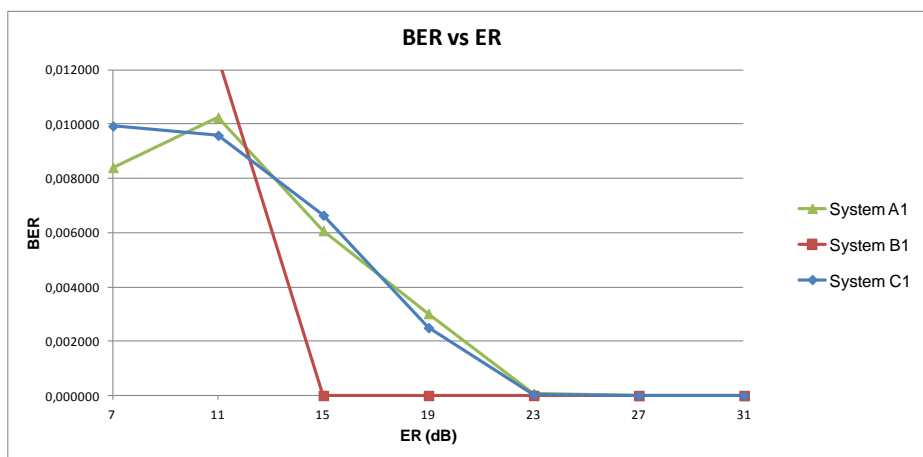


Figure 5.5 BER vs ER representation

Figure 5.5 reflects that systems A₁ and C₁ have a better performance when ER level is under 15dB. From that value system B₁ sharply gets a value of BER=0. Conversely the threshold fixed for system C₁ and A₁ having a BER=0 is ER=23dB.

Following figures show the similar behaviour and trend lines of predistortion systems using a ER=120dB (blue graphics) and ER=30 (red graphics).

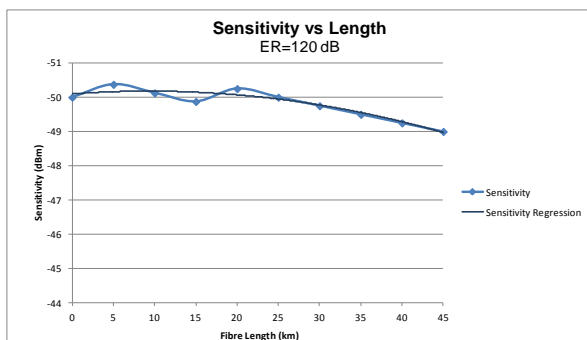


Figure 5.6 System A₁: Sensitivity vs Fibre Length representation

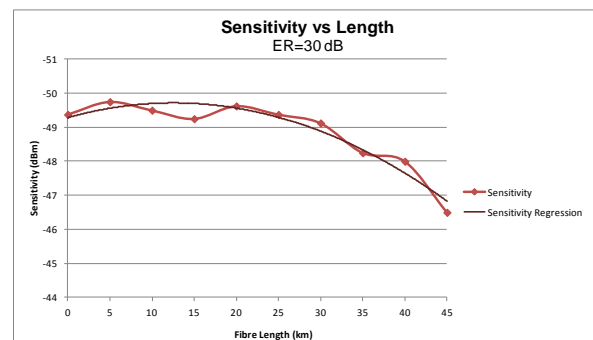


Figure 5.7 System A₁: Sensitivity vs Fibre Length representation

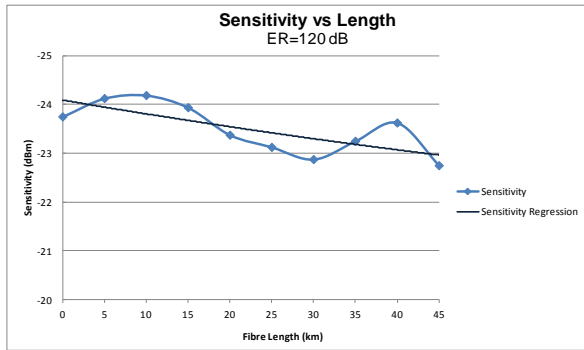


Figure 5.8 System B₁: Sensitivity vs Fibre Length representation

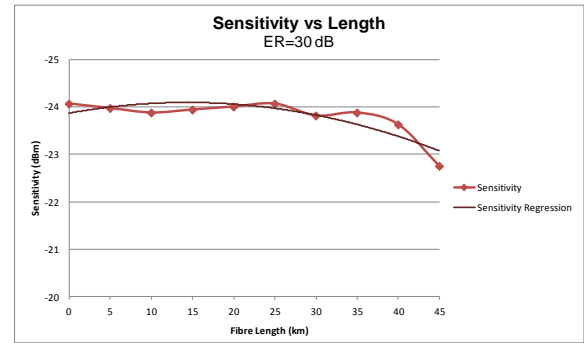


Figure 5.9 System B₁: BER vs Fibre Length representation

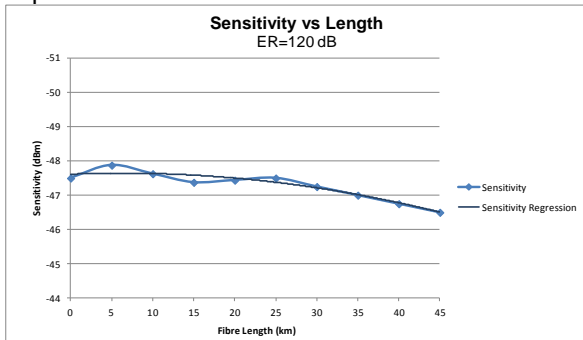


Figure 5.10 System B₁: Sensitivity vs Fibre Length representation

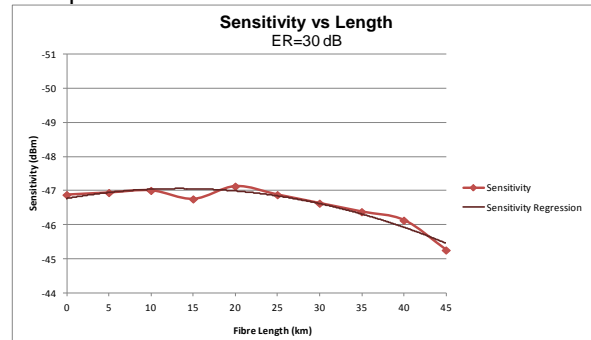


Figure 5.11 System B₁: BER vs Fibre Length representation

Trend lines of conventional oIQ systems with high ER value can be seen in annex C, Sensitivity vs. fibre length results with ER=30 are not shown due to not meeting the required BER even in the B2B case (L=0km).

Chapter 6. Environmental Impact

Overall, the introduction of OFDM in PONs is regarded as a non very energetically efficient solution as it requires the introduction of powerful DSP systems. It, nevertheless, can be argued that this complexity will be required anyhow if one wants to scale to higher and higher velocities, while OFDM may provide an efficient use of the network through its unique features of network reconfigurability and dynamic capacity assignment with high levels of granularity. Moreover, increased reach and user count per OLT in the PON reduces the number of required central offices and energy consuming equipment.

On top of that the predistortion techniques here proposed may allow for energy savings in PONs if used in the user terminals by reducing the DC voltage required. Also the optical integrated circuit required is simpler which leads to reduced environmental impact and energy consumption in its fabrication.

Chapter 7. Conclusions

The main goal of this master thesis is the introduction of a new type of modulation for optical networks based on ***predistortion***. So, complete analytical derivations justifying and describing the new predistortion OFDM optical systems have been included.

Simulation scenarios Matlab cosimulation feature of VPI for up to 6 different optical OFDM systems, including predistortion transmitters, have been developed. These systems have included both conventional oIQ and the new predistortion oIQ transmitter and 3 different types of receivers, namely direct-detection, basic heterodyne coherent detection and conventional homodyne coherent detection. When using DD, modified oIQ transmitters including SSB modulation of an electrical tone were included in both transmitters for providing an optical carrier at a guard distance for direct-detection.

Extensive simulations have been carried out in order to test the predicted performances and to compare them with other alternatives for optical OFDM transmission systems.

A TCL code has been implemented for automatic obtaining of sensitivity vs. fibre length curves with VPI. By choosing the proper attenuation change step and the proper margin around the target BER for stopping the search has allowed to plot and compare the sensitivity vs. length curves for the 6 optical OFDM systems.

The main conclusions stemming from the comparison have been:

- In case of very high ER values ($ER=120\text{dB}$) in the MZM, predistortion oIQ transmitters perform very similarly to conventional oIQ transmitters with sensitivities around -50 dBm , -46 dBm and -24 dBm for conventional homodyne coherent, basic heterodyne coherent and direct detection receivers respectively and maximum 1 dB penalty fiber lengths of roughly 45 Km.
- For realistic ER values (30 dB) conventional oIQ transmitters present very poor performances even in the B2B case while predistortion oIQ transmitters show less than 1 dB sensitivity penalty with respect to the high ER case. The DD receiver is seen to be the most resilient to the loss of ER, keeping the maximum 1 dB penalty reach around 45 Km, while a small reduction to 40 Km is observed in the basic heterodyne receiver. Conventional homodyne coherent receiver is the most sensitive to ER reduction with a maximum reach of 35 Km. for $ER=30\text{ dB}$.
- The tests of the oIQ system for various ER values has revealed that a with the two types of coherent receiver here considered a minimum ER is around 20 dB while with the direct detection a little less than 15 dB could be used for a $BER=10^{-3}$.

These results confirm the potential of predistortion techniques to be applied in the transmitters of optical OFDM systems.

Summarizing, as compared to conventional oIQ transmitters, a predistortion oIQ transmitter:

1. Provides cost savings because the integrated circuit required (DD-MZM) is composed of just one MZ interferometer instead of 3 as in the conventional oIQ and therefore it is simpler to fabricate leading to both reduced fabrication cost and better quality circuits (i.e. higher ERs). In addition, it is easier to operate and more energy efficient, since it does not require a bias voltage to operate, while the conventional oIQ requires adjustment of 3 bias voltages. For these reasons the predistortion oIQ shows potential as ONU transmitter for the uplink.

2. Does not add complexity to the OFDM transmitter because the predistortion functions may be added to the DSP part.
3. Provides similar performances for high (unrealistic) ER values, and allows improving the performances for low (realistic) ER values.

Since this is the first work where the proposal of oIQ transmitters has been studied, there are many open issues worth further analysis, such as for example:

- To go deeper on the characterization and optimization of predistortion oIQ transmitters by testing performances against parameters such as QAM level, FFT size, CP insertion, Carrier to Signal Power Ratio (CSPR), etc.
- To study the effect of phase noise with realistic laser linewidths and to design and analyze proper phase noise compensation techniques.
- To insert the predistortion function inside the matlab coding and assess performances against ADC/DAC limitations.
- To simulate point-to-multipoint scenarios based on predistortion oIQ.
- Prove the predistortion oIQ transmitter in a lab experiment.

Acronyms

3G	Third Generation in cell-phone technology
4QAM	4 Quadrature Amplitude Modulation
Accordance	A Novel OFDMA-PON Paradigm for Ultra-High Capacity Converged Wireline-Wireless Access Networks
APD	Avalanche Photodiode
B2B	Back to Back
BER	Bit Error Rate
CD	Chromatic Dispersion
COH D	Coherent Detection
CP	Cyclic Prefix
CW	Continuous Wave
DAC/ADC	Digital to Analogue Converter / Analogue to Digital Converter
DC	Direct Current
DD	Direct Detection
DD-MZM	Dual Drive – Mach-Zehnder Modulator
DFB	Distributed Feedback laser
DFT	Discrete Fourier Transform
DSP	Digital Signal Processor
ECL	External Cavity Lasers
eIQ	Electrical Inphase / Quadrature
EO	Electro-optic effect
EPON	Ethernet Passive Optical Network
ER	Extinction Ratio
EU	European Union
EVM	Error Vector Magnitude
GPON	Gigabit Passive Optical Network
ICI	Inter-Carrier Interference
IFFT/FFT	Inverse Fast Fourier Transform / Fast Fourier Transform
IM	Intensity Modulation
IM/DD	Intensity Modulation / Direct Detection Systems
IQ	Inphase / Quadrature
ISI	Inter-Symbol Interference
ITU	International Telecommunication Union
LO	Local Oscillator
LOS	Line of Sight
LPF	Low Pass Filter
LTE	Long Term Evolution
MZM	Mach-Zehnder Modulator
NDSF	Non-Dispersion-Shifted Fibre
NGPON	New Generation Passive Optical Networks
NP	Null Point
OFDM	Orthogonal Frequency Division Multiplexing
OFDMA	Orthogonal Frequency Division Multiplexed Access
oIQ	Optical Inphase / Quadrature
OLT	Optical Line Termination
ONU	Optical Network Unit
OTR	Optical To Radiofrequency Module
PIN	PN Junction with Isolation Region photodiode
PON	Passive Optical Networks
PRBS	Pseudo Random Binary Sequence
QP	Quadrature Point
RF	Radiofrequency
RTO	Radiofrequency To Optical Module
RX	Receiver
SSB	Single Side Band
SM	Single Mode

TCL/TK	Tool Comand Language / Tool Kit
TDM	Time Division Multiplexing
TDMA	Time Division Multiplexed Access
TETRA	Terrestrial Trunked Radio
TX	Transmitter
VPI	Virtual Photonics Inc.
WDM	Wavelength Division Multiplexing
Wi-Fi	Wireless Fidelity
WiMAX	Worldwide Interoperability for Microwave Access

Bibliography

- [1] William Shieh and Ivan Djordjevic, *Orthogonal Frequency Division Multiplexing for Optical Communications*, (1st edition, 2010).
- [2] Scott T. Wilkinson, *PON Today & Tomorrow, Next-Generation PON Architectures and Their Impact on the OSP*.
- [3] Cristóbal Manuel Romero Vidal Supervisor: María Concepción Santos, *Optimization of optical OFDM systems (January 2012)*.
- [4] <http://www.ict-accordance.eu/>
- [5] Uma Shanker Jha, Ramjee Prasad, *OFDM towards fixed and mobile broadband wireless access*.
- [6] Jean Armstrong (Senior Member IEEE), *OFDM for Optical Communications*.
- [7] Sander L. Jansen, *SC341 OFDM for Optical Communications*.
- [8] S. Kumar, *Impact of Nonlinearities on Fiber Optic Communications, Optical and Fiber Communications Reports 7*.
- [9] Fribiz Tian, *Optical Time Division Multiplexing Technology*.
- [10] <http://www.worldoflasers.com/laserproperties.htm>
- [11] Brendon J. C. Schmidt, Arthur James Lowery, Senior Member, IEEE, and Jean Armstrong, Senior Member, IEEE, *Experimental Demonstrations of Electronic Dispersion Compensation for Long-Haul Transmission Using Direct-Detection Optical OFDM*.
- [12] Konstantinos Kanonakis and Ioannis Tomkos, Heinz-George Krimmel and Frank Schaich, Christoph Lange and Erik Weis, Juerg Leuthold and Marcus Winter, Karlsruhe Institute of Technology, Sergio Romero, Pandelis Kourtessis and Milo Milosavljevic, Ivan N. Cano and Josep Prat., *An OFDMA-Based Optical Access Network Architecture Exhibiting Ultra-High Capacity and Wireline-Wireless Convergence*.
- [13] CISCO White Paper, *Fiber Types in Gigabit Optical Communications*.
- [14] Gerd Keiser, *Optical Fiber Communications (3^d edition)*.
- [15] P. S. Cho, G. Harston, C. Kerr, A. Greenblatt, A. Kaplan, Y. Achiam, and I. Shpanzer, "IEEE Photon. Technol. Letts., vol. 16, no. 7, pp. 1727-1729, July, 2004, *Coherent homodyne detection of BPSK signals using timegated amplification and LiNbO3 optical 90° hybrid*.
- [16] *VPItransmissionMaker* help module.

ANNEXES

A. Diode Laser Definition

Its acronym defined it as Light Amplification by Stimulated Emission of Radiation, generally speaking it is a device that creates and amplifies a narrow, intense beam of coherent light. A coherent light is achieved by generating photons with the same phase, polarization and direction.

This device is the main and most important part of the optical transmitter because it generates the optical signal or optical carrier where the modulated data will be imposed. It is important to notice that light-generation process occurs in certain materials due to recombination of electrons and holes in p-n junctions.

The most important materials used to build a laser are liquids, crystals, gas or semiconductors. Thus they will be applied different methods in order to force the electron to the excited state (farthest location or level from the atom's core).

Stimulated Emission

Stimulated Emission mechanism allows generating an amplified output in a light source by applying different conditions listed below.

First of all raising the atomic population from ground state (N_1 , with energy E_1) to the excited state (N_2 , with energy E_2) is required. As in normal conditions N_1 is larger than N_2 , is mandatory to obtain what is called **population inversion**, represented in (0.1).

$$N_2 > N_1 \quad (0.1)$$

In order to achieve this inversion, is compulsory to add an external energy source. The light generated has to be emitted at the same wavelength and with the same energy of the resultant photons that will be sent through the system. In Figure 0.1 is shown the stimulated emission's electron-hole scheme. In the image it is observed how by each generated photon, an electron descends from higher to lower level producing a photon plus the injected one, therefore emitting two photons and producing light amplification at the output.

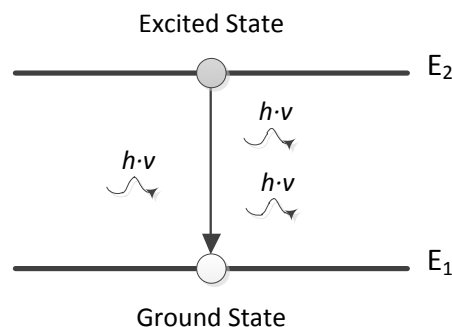


Figure 0.1 Stimulated Emission's Scheme

In order to sustain stimulated emission (forming useful laser output) there exist three basic components required in a laser:

- Pump Source
- Active Medium

- Feedback Mirrors

Both pump source and active medium can be implemented in different forms, depending on the type of laser. In the Fabry-Perot semiconductor laser, the pump source is an electrical current and the active material is found as a solid. In Figure 0.2 is shown a basic Fabry-Perot semiconductor laser scheme.

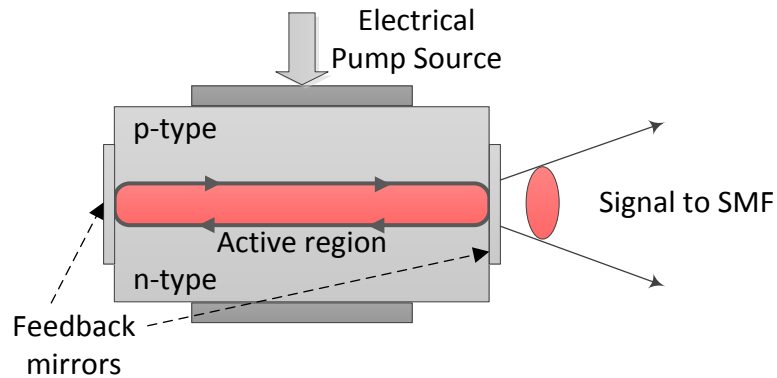


Figure 0.2 Detailed Fabry-Perot semiconductor laser Scheme

The electrical pump source (bias) flows through the p-n junction and stimulates the recombination of electron and holes, leading to the generation of photons [1].

Linewidth and Monochromatic Light Generation

As it has been defined before a laser aims to generate a coherent, monochromatic and high concentrated light.

Monochromatic refers to the generation of photons with the same energy. The photon's energy is defined as follows:

$$E_{ph} = \frac{h \cdot c}{\lambda} \quad (0.2)$$

The different parameters in equation (0.2) are:

- Planck's constant $\rightarrow h = 6.626068 \cdot 10^{-34} \frac{\text{m}^2 \cdot \text{kg}}{\text{s}}$.
- Speed of light constant $\rightarrow c = 3 \cdot 10^8 \frac{\text{m}}{\text{s}}$.
- Wavelength of the photon $\rightarrow \lambda = \lambda_i$.

In order to obtain the same photon's energy the variable parameter, wavelength, has to be fixed. Therefore all different generated photons have to be on the same wavelength and so the laser source will have to emit a single spectral colour.

In practical a laser generates light in a very narrow band around a single and central wavelength hence it does not generate a pure monochromatic light. In frequency domain the interval or range around the central frequency is called linewidth or laser bandwidth and it defines the laser degree of monochromaticity [9].

B. PIN Photodiode

It is the most common photodiode and it consists of p and n regions separated by a very lightly n -doped intrinsic region i . When a photon flux Φ penetrates into a semiconductor it will be absorbed as it progresses through the material.

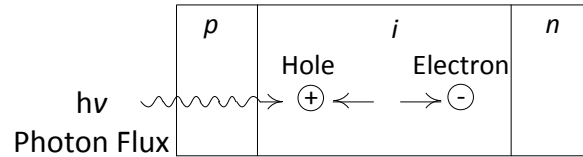


Figure 0.3 Photon flux passing through photodiode material

Having P_{in} as the input of the photodiode, $\alpha_s(\lambda)$ as the photon absorption coefficient at a wavelength λ and x as the distance where the photon flux passes through the semiconductor the power level $P(x)$ is obtained at a distance x into the material in the expression (0.3)

$$P(x) = P_{in} \cdot e^{-\alpha_s \cdot x} \quad (0.3)$$

When an incident photon has energy greater than or equal to the band-gap energy E_g of the semiconductor material, the photon can give up its energy and excite an electron from the valance band to the conduction band, generating free electron-hole pairs which act as photocurrent carriers, Figure 0.4.[14]

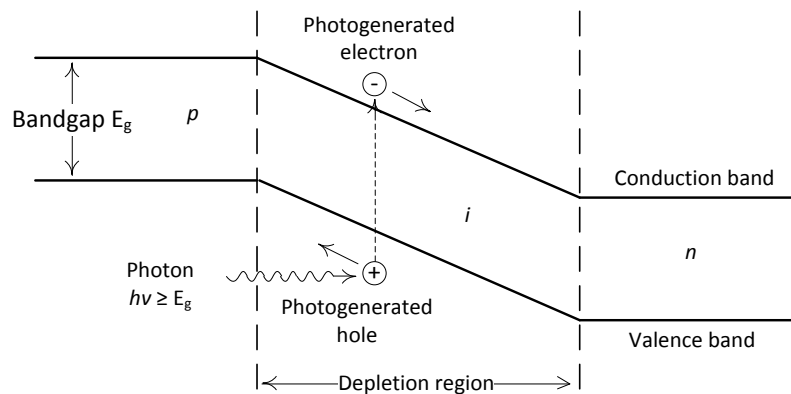


Figure 0.4 Energy-band's diagram for pin photodiode

C. oIQ Systems

All these systems have the same setting parameters at the transmitter side. Important modules are Mach Zehnder modulators (section 1.2.2.4). Both MZMs work at Null Point, what it means the optical carrier at f_{REF} is not visible in yellow figures.

Inevitably the fact of changing ER value affects directly the resultant optical signal. When ER has a low value as it is 30 dB the phase modulation inside MZMs is disturbed due to the imbalance between branches. This introduces negative effects over the resultant signal as it is the chirp.

All the figures in the three following systems have been simulated with an ER=120dB, what it means the signal weight distributed into the two branches of each MZMs is nearly the same.

oIQ / Hybrid 90° COHD B2B System's Description

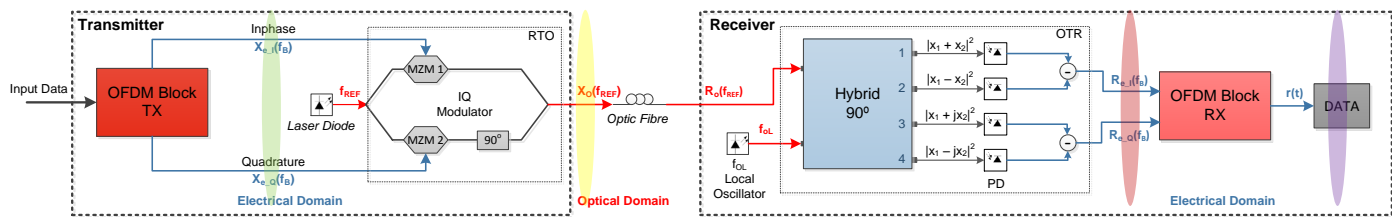


Figure 0.5 OFDM oIQ with Homodyne Hybrid 90° Coherent Detection Scheme

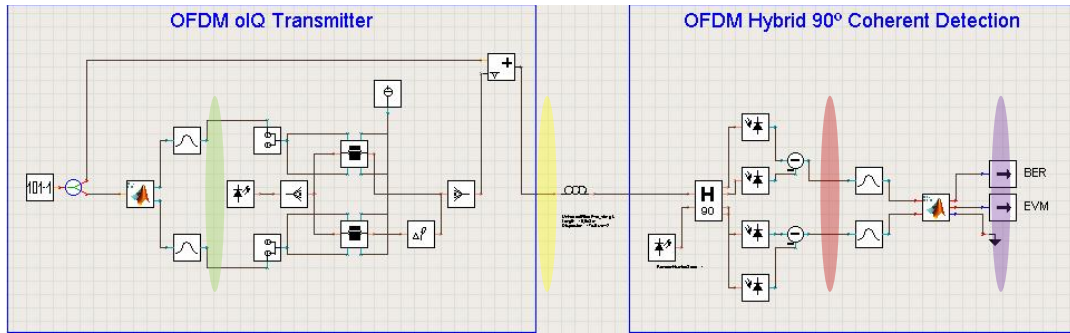


Figure 0.6 OFDM oIQ with Homodyne Hybrid 90° Coherent Detection Scheme in VPI. Shown in Figure 0.5 or Figure 0.6 the **Input Data** is introduced into the OFDM Coder Block in order to map, modulate and encode the input signal. The modulation used inside the OFDM Block is a 4QAM, after these symbols are encoded as an OFDM symbol (to know more about the processes of an OFDM coder, read sections 1.1.1.3 and 3.2.1). These outputs are the electrical OFDM signal's components $X_{e_I}(f_B)$ and $X_{e_Q}(f_B)$, Figure 0.7.

The following step is converting $X_{e_I}(f_B)$ and $X_{e_Q}(f_B)$ in an optical signal by phase modulating each other with a different MZM having a phase shift between them of 90°. The optical carrier where the input data will be sent through the channel is injected by a laser. This laser emits an optical carrier located around the reference frequency of the fibre, $f_{REF} = 193.1 THz$ (in section 1.2.2.2 there is information about the chosen reference frequency).

The output's optical signal coming from the RTO block is $X_o(f_{REF})$, Figure 0.8. This optical base band signal is ready to be introduced into the channel or SM optical fibre.

Once the optical signal arrives at the receiver side is introduced inside the hybrid 90° (section 1.2.2.5). This hybrid is a coupler that mixes received signal with and auxiliary carrier located at the same reference frequency due to this is a homodyne system and so the signal is located at the optical base band.

As seen in Figure 0.9 System A: $R_{e_l}(f_B)$ signals $R_{e_l}(f_B)$ and $R_{e_o}(f_B)$ have been converted to base band in electrical domain with the OTR block.

Then the signal is prepared to enter inside the OFDM Decoder Block in order to recover the original sent signal (there is more information about OFDM decoder process in sections 1.1.1.3 and 3.2.2).

$ER = 120dB$ and $L=0 km$

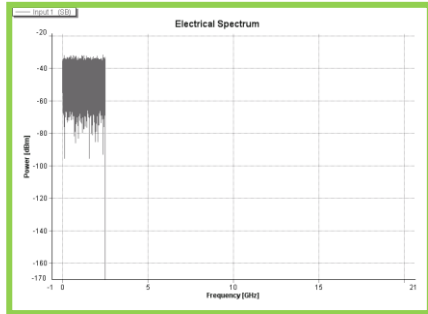


Figure 0.7 System A: $X_{e_l}(f_B)$

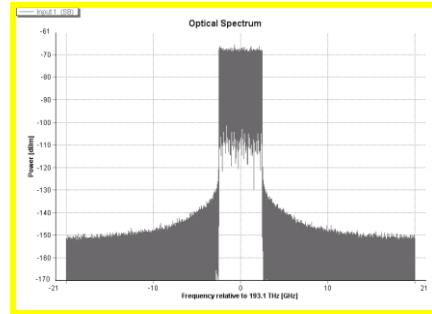


Figure 0.8 System A: $X_o(f_{REF})$

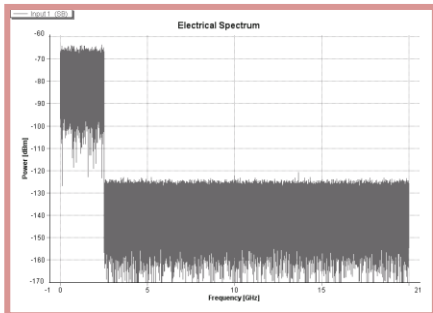


Figure 0.9 System A: $R_{e_l}(f_B)$

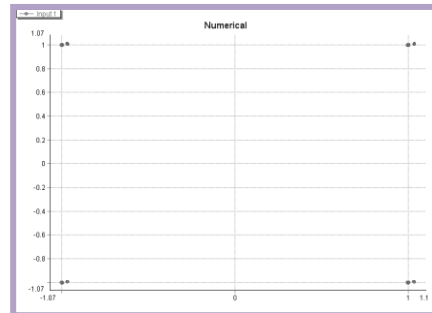


Figure 0.10 System A: Constellation Diagram, BER=0

The obtained BER's value in order to conform the constellation diagram is null. In Figure 0.10 a replica of the symbol with a deviation of (0.03, 0.01) is observed, considering this symbols inside each of the 4QAM symbols' area.

oIQ plus SSB modulated Tone / DD: B2B System's Description

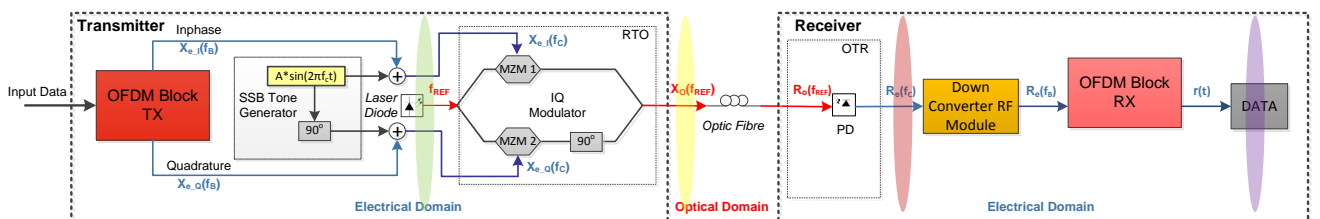


Figure 0.11 OFDM oIQ plus SSB modulated Tone with Direct Detection Scheme

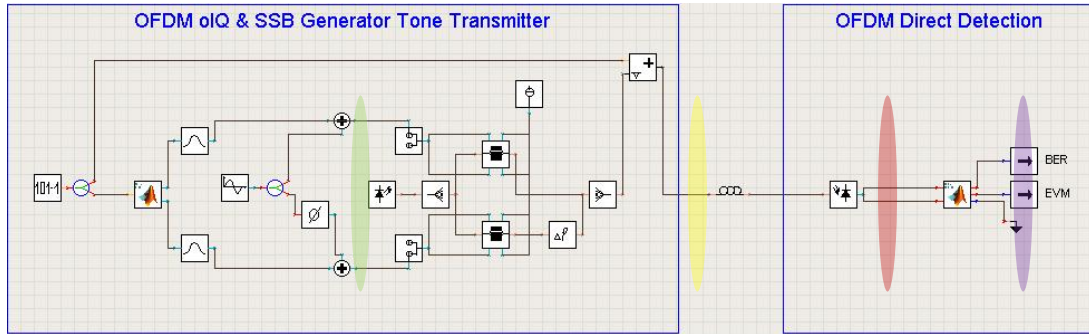


Figure 0.12 OFDM oIQ plus SSB modulated with Direct Detection Scheme in VPI

As seen in Figure 0.11 or Figure 0.12 the **Input Data** is introduced into the OFDM Coder Block following the same process as in the system above. Its outputs are the electrical OFDM signal's components $X_{e_I}(f_B)$ and $X_{e_Q}(f_B)$. These signals are added to a Single Side Band tone at $f_c=15\text{GHz}$, as shown in Figure 0.13.

The following step is converting $X_{e_I}(f_B)$ and $X_{e_Q}(f_B)$ in an optical signal by phase modulating each other in the same way as in the system above and with an optical carrier at the reference frequency of the fibre, $f_{REF}=193.1\text{THz}$ (in section 1.2.2.2).

Now the resultant optical signal is formed by the electrical packet at the reference frequency and an optical auxiliary carrier at 15 GHz, in Figure 0.14 $X_o(f_{REF})$ is represented. This optical base band signal plus the injected auxiliary carrier are ready to be introduced into the SM optical fibre.

Once the optical signal arrives at the receiver side is introduced directly inside the photodiode, direct detection. This photodetector converts the optical signal into an electrical one as explained in section 1.2.2.3. The obtained signal is an electrical side band signal located at $f_c=15\text{GHz}$, as shown in Figure 0.15. As this signal is not in base band it has to be down converter by adding an additional block as seen in Figure 0.11.

Then the signal is prepared to enter inside the OFDM Decoder Block in order to recover the original sent signal (OFDM decoder process information is in sections 1.1.1.3 and 3.2.2).

$ER = 120\text{dB}$ and $L=0\text{ km}$

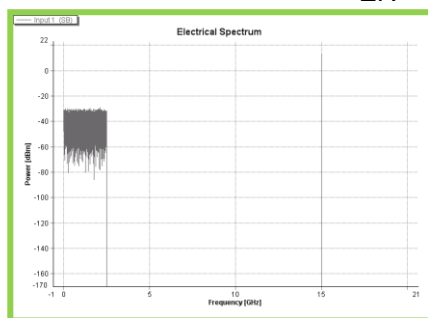


Figure 0.13 System B: $X_{e_I}(f_B)$ & SSB tone at 15GHz

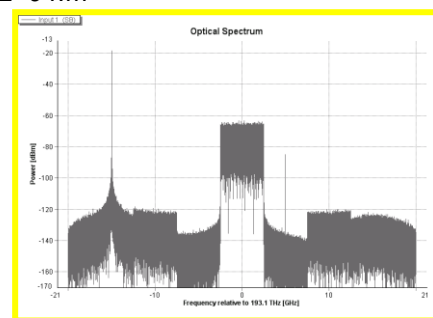


Figure 0.14 System B: $X_o(f_{REF})$

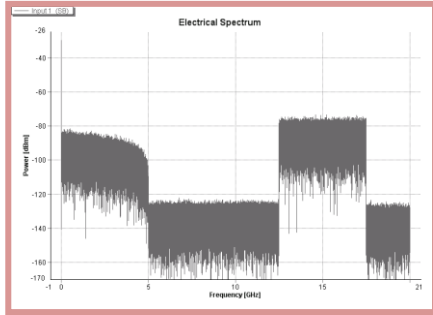


Figure 0.15 System B: $R_e(f_B)$

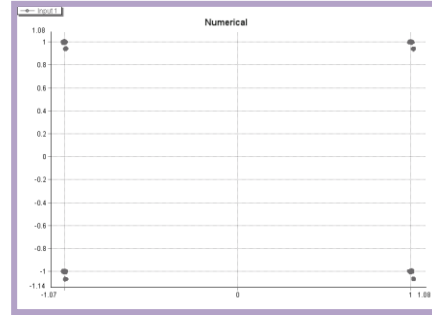


Figure 0.16 System B: Constellation Diagram, BER=0

The obtained BER's value in order to conform the constellation diagram is null. In Figure 0.16 is observed a replica of the symbol with a deviation of (0.001, -0.06), considering this symbols inside each of the 4QAM symbols' area.

oIQ / Basic Heterodyne COHD: B2B System's Description

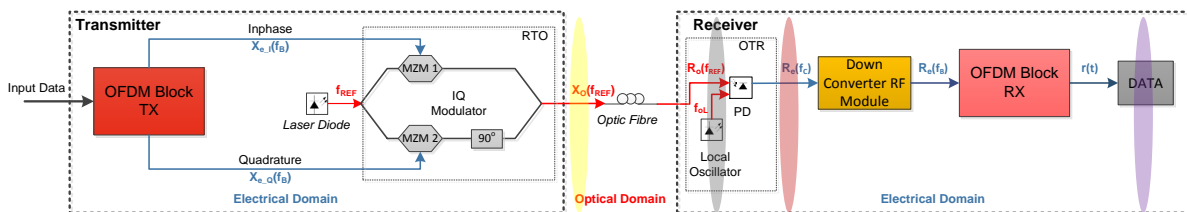


Figure 0.17 OFDM oIQ with Basic Heterodyne Coherent Detection Scheme

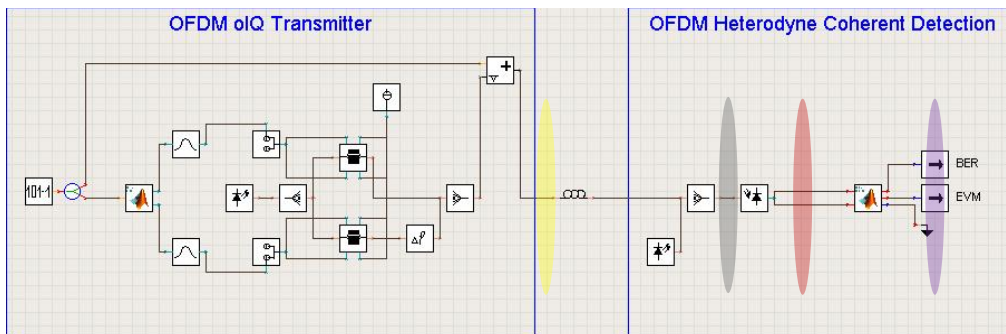


Figure 0.18 OFDM oIQ with Heterodyne Coherent Detection Scheme

According to Figure 0.17 or Figure 0.18 the **Input Data** is introduced into the OFDM Coder Block following the same process as in section above. Its outputs are the electrical OFDM signal's components $X_{e_I}(f_B)$ and $X_{e_Q}(f_B)$.

The following step is converting $X_{e_I}(f_B)$ and $X_{e_Q}(f_B)$ in an optical signal by phase modulating each other in the same way as in section above and with an optical carrier at the reference frequency of the fibre, $f_{REF}= 193.1 THz$ (in section 1.2.2.2).

The output's optical signal coming from the RTO block is $X_o(f_{REF})$, Figure 0.19. This optical base band signal is ready to be introduced into the channel or SM optical fibre.

Once the optical signal arrives at the receiver side is introduced into a photodiode together with an auxiliary carrier or local oscillator generating lorentzian signal at $f_c=15GHz$, Figure 0.20. This auxiliary carrier addition produces a frequency shift into the resultant electrical signal, $R_e(f_c)$, moving the received electrical packet to 15GHz, Figure 0.21.

In order to introduce $R_e(f_c)$ into the OFDM Decoder Block, it has to be down-converted to base band with the module in Figure 0.17.

Then the signal is prepared to enter inside the OFDM Decoder Block in order to recover the original sent signal (OFDM decoder process information is in sections 1.1.1.3 and 3.2.2).

$ER = 120\text{dB}$ and $L=0\text{ km}$

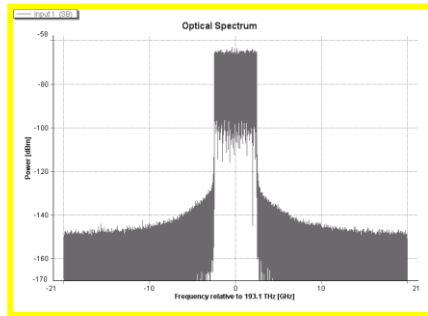


Figure 0.19 System C: $X_o(f_{REF})$

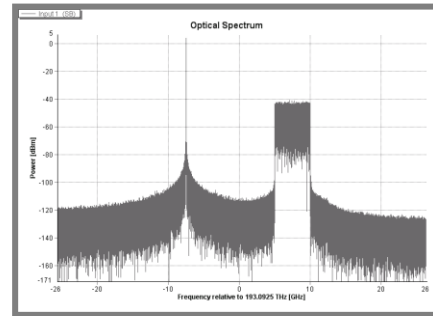


Figure 0.20 System C: $X_o(f_{REF})$ plus the auxiliary carrier at 15 GHz from $X_o(f_{REF})$

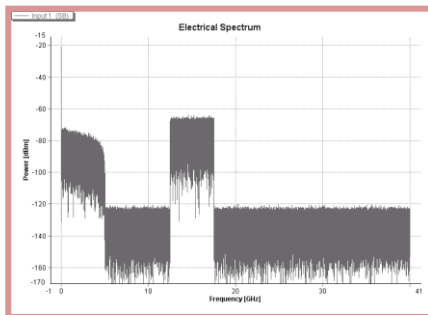


Figure 0.21 System C: $R_e(f_B)$

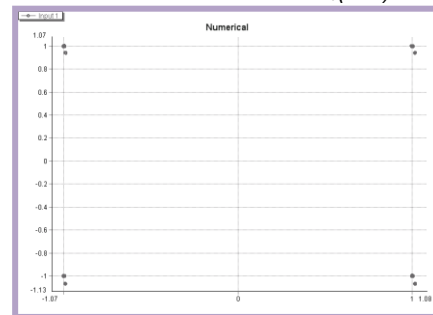


Figure 0.22 System C: Constellation Diagram

The obtained BER's value in order to conform the constellation diagram is null. In Figure 0.22 A replica of the symbol with a deviation of (0.001, -0.05) is observed, considering this symbols' area inside each of the 4QAM symbols' area.

oIQ Results: Systems A_2 / B_2 / C_2

Sensitivity vs. Fibre Length

In order to obtain representative trend lines when analysing the systems' sensitivity versus fibre length the graphics have been trunked to a length. The reason of doing it is because of considering meaningful the sensitivity curve until it decays approximately 1dB.

Surprisingly this length is the same for A, B and C systems; its value is $L_{\text{fibre}}=45\text{ km}$.

Comparing the initial and most constant sensitivity value of the three different systems, system B (Figure 0.24) requires a very high value of $S_B=-23\text{ dBm}$ while in systems A and C they are around $S_A=-50\text{ dBm}$ and $S_C=-47.5\text{ dBm}$ respectively.

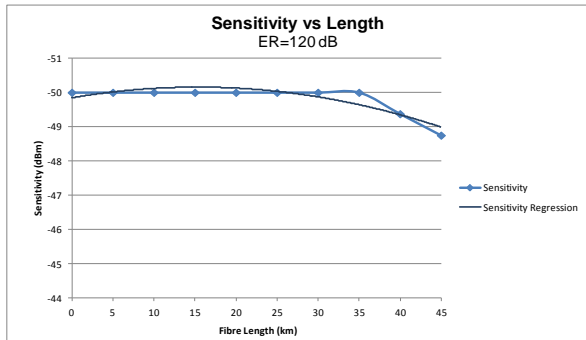


Figure 0.23 System A2: Sensitivity vs Length representation

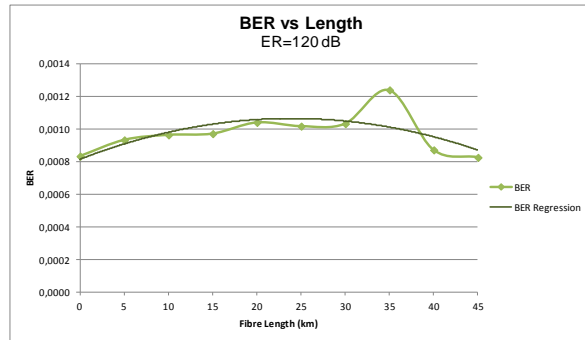


Figure 0.24 System A2: BER vs Length representation

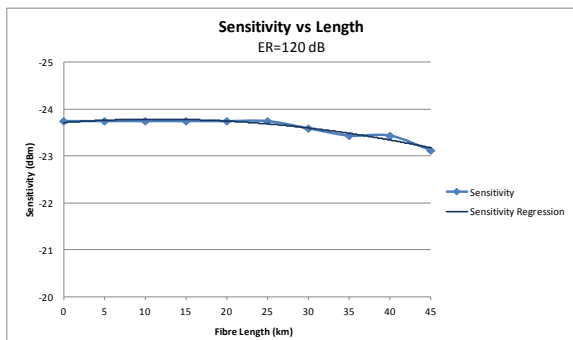


Figure 0.25 System B2: Sensitivity vs Fibre Length representation

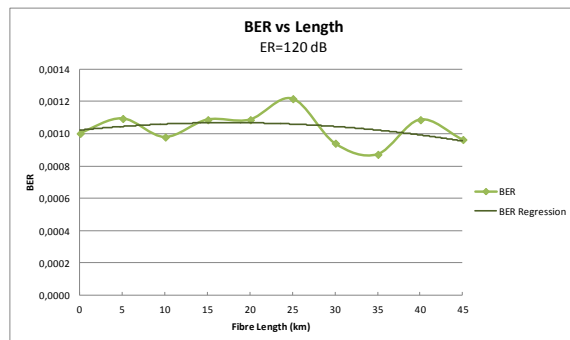


Figure 0.26 System B2: Sensitivity vs Fibre Length representation

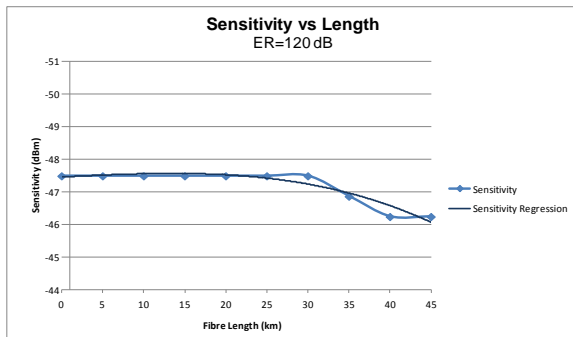


Figure 0.27 System C2: Sensitivity vs Fibre Length representation

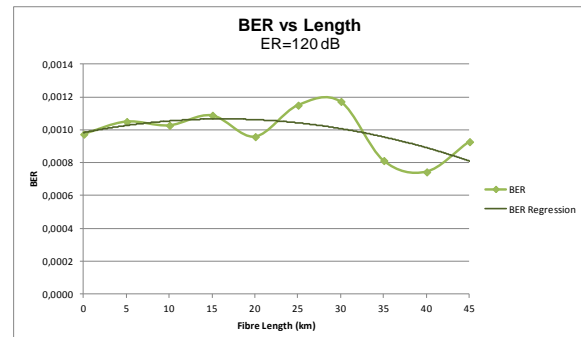


Figure 0.28 System C2: BER vs Fibre Length representation

Regarding the bit error rate performance when incrementing the fibre length, the most stable system is A

ER variation

When changing the ER value to a lower one, data reception is worsened in all the oIQ systems as shown in Figure 0.29, Figure 0.30 and Figure 0.31.

Now ER = 30dB and the eye diagram shows again the chirp effect with distances of 4,35, 7,49 and 7,39 (systems A, B and C respectively). As expected they are not meeting the BER's requirement of $1 \cdot 10^{-3}$ (before FEC); their obtained values are BER~0.00188.

ER = 30dB and L=0 km

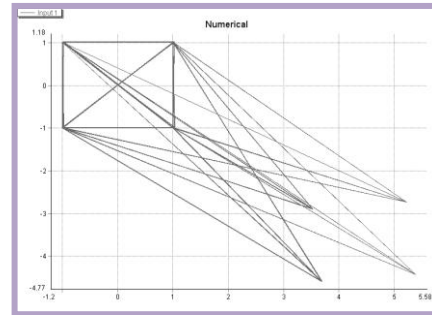
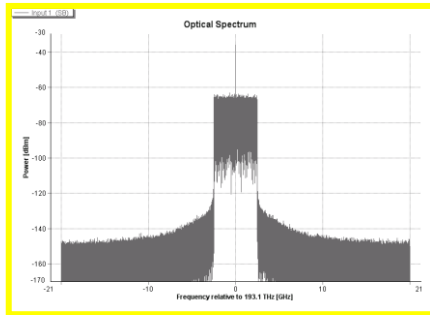


Figure 0.29 System A: $X_o(f_{REF})$ and Eye Diagram, BER=0.00188

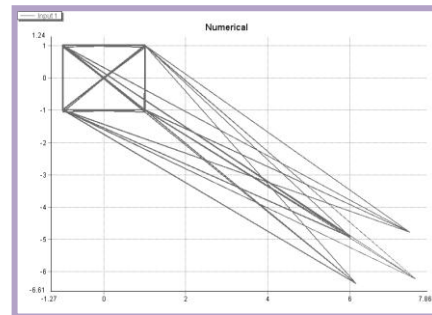
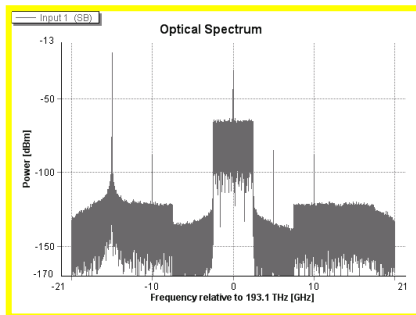


Figure 0.30 System B: $X_o(f_{REF})$ and Eye Diagram with BER=0.00187

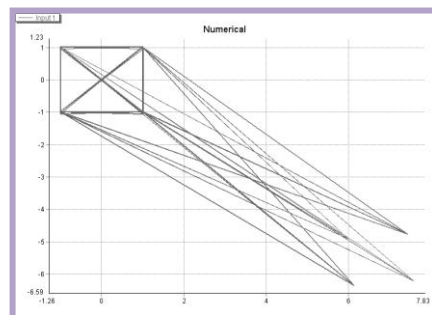
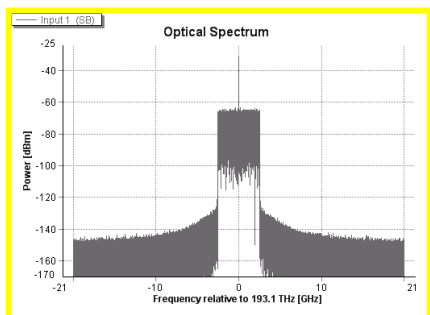


Figure 0.31 System C: $X_o(f_{REF})$ and Eye Diagram with BER=0.00187

D. Tcl/tk Script

```
# tcl-script for Optimization

# get platform

set OS $tcl_platform(os)

# save file name

set saveFile1
c:/BLANCA_6/Simulacions/oIQ_CarrierRX/10_16bits_ER30.dat

# initialization

set prec 6e-4

set lim 1e-3

# clean the save file

set fileID1 [open $saveFile1 w]

close $fileID1

# search for the laser power until a BER <= 1.0e-9

for {set L 0} {$L<100000} {incr L 5000} {

setstate UniversalFiberFwd_vtmgl Length $L

set a 0

set b 0

set startAtt 40

set deltaAtt 5.

set cont 0

# set the laser power

    initialize Attenuator Attenuation

    setstate Attenuator Attenuation $startAtt

# execute the simulation

run 1

wrapup

# get the BER value

    set BER [statevalue BERcalculator InputValue]

    set EVM [statevalue EVMcalculator InputValue]

    set PRX [statevalue PRXcalculator InputValue]
```

```

while { $BER > $lim + $prec/2 || $BER < $lim - $prec/2 } {
  if { $BER > $lim + $prec/2 } {
    set startAtt [expr $startAtt - $deltaAtt ];
    set b -1;
    initialize Attenuator Attenuation
    setstate Attenuator Attenuation $startAtt
    run 1
    wrapup
    set BER [statevalue BERcalculator InputValue]
    set EVM [statevalue EVMcalculator InputValue]
    set PRX [statevalue PRXcalculator InputValue]
    if { $BER < $lim - $prec/2 } {
      set a 1;
    }
  } elseif { $BER < $lim - $prec/2 } {
    set startAtt [expr $startAtt + $deltaAtt ];
    set a 1;
    initialize Attenuator Attenuation
    setstate Attenuator Attenuation $startAtt
    set prova $BER
    run 1
    wrapup
    set BER [statevalue BERcalculator InputValue]
    set EVM [statevalue EVMcalculator InputValue]
    set PRX [statevalue PRXcalculator InputValue]
    if { $BER > $lim - $prec/2 } {
      set b -1;
    }
  }
}

if { $a*$b < 0 } {

```

```
    set deltaAtt [expr $deltaAtt / 2];
    set a 0;
    set b 0;
  }
}
set fileID1 [open $saveFile1 a]
puts $fileID1 "$L $startAtt $PRX $BER $EVM"
close $fileID1
}
```